

RESEARCH

Open Access



EMP3 sustains oncogenic EGFR/CDK2 signaling by restricting receptor degradation in glioblastoma

Antoni Andreu Martija^{1,2,3} , Alexandra Krauß^{1,2,4}, Natalie Bächle^{1,2,3,5}, Laura Doth^{1,2,3}, Arne Christians^{6,7}, Damir Krunic⁸, Martin Schneider⁹, Dominic Helm⁹, Rainer Will¹⁰, Christian Hartmann⁶, Christel Herold-Mende¹¹, Andreas von Deimling^{1,2} and Stefan Pusch^{1,2*} 

Abstract

Epithelial membrane protein 3 (EMP3) is an *N*-glycosylated tetraspanin with a putative trafficking function. It is highly expressed in isocitrate dehydrogenase-wild-type glioblastoma (IDH-wt GBM), and its high expression correlates with poor survival. However, the exact trafficking role of EMP3 and how it promotes oncogenic signaling in GBM remain unclear. Here, we show that EMP3 promotes EGFR/CDK2 signaling by regulating the trafficking and enhancing the stability of EGFR. BioID2-based proximity labeling revealed that EMP3 interacts with endocytic proteins involved in the vesicular transport of EGFR. EMP3 knockout (KO) enhances epidermal growth factor (EGF)-induced shuttling of EGFR into RAB7 + late endosomes, thereby promoting EGFR degradation. Increased EGFR degradation is rescued by the RAB7 negative regulator and novel EMP3 interactor TBC1D5. Phosphoproteomic and transcriptomic analyses further showed that EMP3 KO converges into the inhibition of the cyclin-dependent kinase CDK2 and the repression of EGFR-dependent and cell cycle transcriptional programs. Phenotypically, EMP3 KO cells exhibit reduced proliferation rates, blunted mitogenic response to EGF, and increased sensitivity to the pan-kinase inhibitor staurosporine and the EGFR inhibitor osimertinib. Furthermore, EGFR-dependent patient-derived glioblastoma stem cells display a transcriptomic signature consistent with reduced CDK2 activity, as well as increased susceptibility to CDK2 inhibition upon EMP3 knockdown. Lastly, using TCGA data, we showed that GBM tumors with high EMP3 expression have increased total and phosphorylated EGFR levels. Collectively, our findings demonstrate a novel EMP3-dependent mechanism by which EGFR/CDK2 activity is sustained in GBM. Consequently, EMP3's stabilizing effect provides an additional layer of tumor cell resistance against targeted kinase inhibition.

Keywords CDK2, EGFR, EMP3, TBC1D5, Glioblastoma

*Correspondence:

Stefan Pusch

s.pusch@dkfz-heidelberg.de

Full list of author information is available at the end of the article



© The Author(s) 2023. **Open Access** This article is licensed under a Creative Commons Attribution 4.0 International License, which permits use, sharing, adaptation, distribution and reproduction in any medium or format, as long as you give appropriate credit to the original author(s) and the source, provide a link to the Creative Commons licence, and indicate if changes were made. The images or other third party material in this article are included in the article's Creative Commons licence, unless indicated otherwise in a credit line to the material. If material is not included in the article's Creative Commons licence and your intended use is not permitted by statutory regulation or exceeds the permitted use, you will need to obtain permission directly from the copyright holder. To view a copy of this licence, visit <http://creativecommons.org/licenses/by/4.0/>. The Creative Commons Public Domain Dedication waiver (<http://creativecommons.org/publicdomain/zero/1.0/>) applies to the data made available in this article, unless otherwise stated in a credit line to the data.

Introduction

Epithelial membrane protein 3 (EMP3) is an *N*-glycosylated tetraspanin implicated in isocitrate dehydrogenase-wild-type (IDH-wt) glioblastoma (GBM) [12, 13, 29, 43]. EMP3 has low expression in the adult brain but among gliomas, it is exclusively highly expressed in IDH-wt GBM [29, 43, 66]. High EMP3 expression is positively associated with poor survival of GBM patients [14, 18, 20, 29, 66]. Studies have shown that EMP3 supports TGF- β signaling in CD44-high GBM cells [29] and induces an immunosuppressive GBM microenvironment characterized by reduced T cell infiltration and increased amounts of M2 macrophages in animal models [12]. In non-glioma cells, EMP3 facilitates the activation of receptor tyrosine kinase (RTK) signaling pathway components, including the epidermal growth factor receptor (EGFR) [13, 23, 63]. This is proposed to occur through EMP3's putative trafficking function, after a yeast two-hybrid screen identified EMP3's interaction with several EGFR trafficking regulators [13]. However, these mechanisms, along with their potential downstream consequences, have not been further elucidated. To date, whether and how EMP3 regulates EGFR trafficking and signaling in IDH-wt GBM are still unclear. At the same time, it is unknown how the glycosylation motifs at asparagine 47 (N47) [13] could possibly regulate or modify EMP3's presumed oncogenic function(s).

Aberrant EGFR activation is frequently observed in IDH-wt GBM [40, 44]. This usually results from *EGFR* gene amplification and/or from mutations that promote constitutive activation of the receptor [24, 47]. Once activated, EGFR undergoes autophosphorylation, thereby stimulating downstream signaling most notably through the PI3K/AKT and MAPK pathways [24]. In non-malignant cells, this signaling cascade is controlled by several homeostatic mechanisms, including endolysosomal degradation of EGFR [2, 9]. After binding to EGF, phosphorylated EGFR is internalized into endosomes and eventually shuttled into lysosomes, leading to receptor degradation and termination of signaling [2]. However, tumor cells can bypass this process by inhibiting receptor internalization, promoting receptor recycling, or attenuating receptor degradation [9, 24, 45]. Such mechanisms contribute to the ability of GBM cells to sustain EGFR overactivation and its downstream oncogenic effects. It is critical to understand how putative trafficking regulators like EMP3 participate in this process, as it may reveal novel strategies aimed at attenuating EGFR resistance to negative feedback regulation.

In this study, we aimed to unravel EMP3's protein-protein interaction (PPI) network and investigate how EMP3 regulates EGFR trafficking in IDH-wt GBM cells. In parallel, we sought to examine the downstream

consequences of silencing EMP3 in a panel of EGFR-dependent GBM cells. To achieve these objectives, we integrated BioID2-based PPI interaction analysis, phosphoproteomics, transcriptomics, and CRISPR/Cas9- and shRNA-based loss of function studies. To demonstrate the potential clinical utility and relevance of our findings, we also investigated how candidate drugs synergize with EMP3 depletion and further validated EMP3's effects on EGFR activity using The Cancer Genome Atlas (TCGA) dataset. Our comprehensive approach identified a novel EMP3-dependent trafficking mechanism that stabilizes EGFR/CDK2 signaling, which subsequently confers IDH-wt GBM cells therapeutic resistance against kinase inhibition.

Materials and methods

Cell culture

U-118 and DK-MG cells were purchased from the American Type Culture Collection (ATCC, Virginia, USA) and the German Collection of Microorganisms and Cell Culture (DSMZ, Braunschweig, Germany), respectively. Both cell lines were authenticated by Multiplexion (Heidelberg, Germany) and checked for mycoplasma contamination by GATC (Ebersberg, Germany). Both cell lines were grown as adherent monolayers and maintained at 37 °C, 5% CO₂ in Dulbecco's Modified Eagle Medium (DMEM) with high glucose, GlutaMAX and pyruvate (Gibco 31966047) supplemented with 10% Fetal Bovine Serum (Gibco 10500-064) and 1% antibiotic-antimycotic (Gibco 15240-062). The glioblastoma stem cell (GSC) lines NCH1425 and NCH644 were obtained from the Department of Neurosurgery of the Heidelberg University Hospital. GSCs were grown as tumor spheroids and maintained in DMEM/F-12 with GlutaMAX (Gibco 31331028) supplemented with B-27 (Gibco 12587010), 20 ng/mL human EGF (Peprotech AF-100-15-100), 20 ng/mL of human FGF-basic (Peprotech 100-18B-250) and 1% antibiotic-antimycotic. All adherent and suspension cells were profiled by whole exome sequencing and copy number profiling by the Department of Neuropathology of the Heidelberg University Hospital. Stably transfected or lentivirally transduced cells were selected and maintained in the same medium supplemented with 0.5 to 1 μ g/mL puromycin (MP Biomedicals 194539) or 4 μ g/mL blasticidin (US Biological Life Sciences B2104-30). Generation of CRISPR/Cas9-edited EMP3 KO cells and other cell lines stably expressing cloned plasmids are further described in the Additional file 1: Materials and Methods.

BioID2-based proximity labeling

Total cell lysates were collected from U-118 cells expressing BioID2 bait constructs and treated with 50 μ M biotin (Sigma-Aldrich B4639) for 18 h. Lysates were subjected to streptavidin pull-downs using Pierce High Capacity Streptavidin Agarose Resin (Thermo Fisher Scientific 20357) following the manufacturer's protocol. Eluates were then subjected to liquid chromatography—tandem mass spectrometry (LC–MS/MS) analysis using the Ultimate 3000 UPLC system directly connected to an Orbitrap Exploris 480 mass spectrometer (Thermo Fisher Scientific). Protein identification and quantification were carried out using MaxQuant version 1.6.14.0 [59] and statistical analysis was performed using Perseus 1.6.14.0 [60]. Network and data visualization were further performed using Cytoscape version 3.9.1 [54] and ProHitsviz [31]. Sample preparation as well as data acquisition and analysis settings are further detailed in the Additional file 1: Supplementary Materials and Methods.

Phosphoproteomic analysis

Total cell lysates were collected from GBM control and EMP3 KO cells lysed with 1% sodium dodecyl sulfate and 1% sodium deoxycholate in 100 mM triethylammonium bicarbonate (TEAB; Thermo Fisher Scientific PI90114) containing protease and phosphatase inhibitors. Lysates were heated at 95 °C for 5 min, sonicated for 5 cycles (35% power for 20 s per cycle), and clarified by centrifugation at 20,000 \times g at 4 °C for 10 min. Proteins were precipitated using chloroform/methanol as previously described [64]. Protein pellets were then resuspended (8 M Urea, 100 mM NaCl, 50 mM TEAB, pH 8.5), followed by reduction in 10 mM DTT for 1 h at 27 °C, alkylation by 30 mM iodoacetamide for 30 min at room temperature in the dark and quenching the reaction by adding additional 10 mM DTT. Samples were subsequently digested by Lys-C at an enzyme:protein ratio of 1:100 for 3–4 h at 30 °C, diluted with 50 mM TEAB to achieve a final urea concentration of 1.6 M, and further digested with trypsin overnight at 37 °C in an enzyme:protein ratio of 1:50. Digestion was stopped by acidification using TFA (0.02% (vol/vol) TFA). Digested peptides were desalted using C18 SepPack cartridges and resuspended in 0.07% (v/v) TFA in 30% (v/v) ACN and fractionated by on-column Fe³⁺-IMAC enrichment on an Ultimate 300 LC system using a previously described method [50]. The two resulting fractions per sample, containing either unphosphorylated or phosphorylated peptides, were desalted by StageTips [49]. Prior to LC–MS/MS analysis the dry peptides were resolved in 50 mM citric acid and 0.1% TFA. LC–MS/MS analysis was performed using the mass spectrometer described above and following the settings

described in the Additional file 1: Supplementary Materials and Methods. Protein quantification and statistical analysis were performed using MaxQuant version 1.6.14.0 [59]. Phosphorylation analysis was performed using Ingenuity Pathway Analysis version 22.0 (Qiagen). Kinase enrichment analysis and upstream kinase prediction were additionally performed using Kinase Enrichment Analysis version 3 [34] and Robust Inference of Kinase Activity version 2.1.3 [65], respectively. Top upstream kinases were visualized by generating dot plots with the ggplot2 R package. Additional details about data acquisition and analysis are further detailed in the Additional file 1: Supplementary Materials and Methods.

Microarray analysis

Total RNA were extracted from U-118, DK-MG, and NCH1425 cells using the Nucleospin RNA kit (Macherey–Nagel) following the manufacturer's instructions. Samples were sent to the Microarray Core Facility (Heidelberg, Germany), which performed quality control followed by microarray hybridization using the Human Clariom S assay (Applied Biosystems). To analyze microarray data, raw CEL files were imported into the Transcriptome Analysis Console software version 4.0.2.15 (Thermo Fisher Scientific). Differentially expressed genes (DEGs) between control and EMP3-depleted cells were identified by filtering for genes with a linear fold-change ≤ -2 (i.e., downregulated) or ≥ 2 (i.e., upregulated) and P -value ≤ 0.05 . DEG lists were then imported into the Ingenuity Pathway Analysis software version 22.0 (IPA, Qiagen). Core analysis was performed on all downregulated and upregulated genes using the default IPA settings in the case of NCH1425. For U-118 and DK-MG, which exhibited more DEGs upon EMP3 depletion than NCH1425, the Species parameter was restricted to “Human” only to improve stringency and confidence. Visualization of top hits using dot plots were performed using the ggplot2 R package. KEGG and Reactome pathway analyses of DEGs and master regulators were performed using the Cytoscape stringAPP plug-in (version 1.7.1). Gene set enrichment analysis was also performed using GSEA version 4.2.3 [57]. Volcano plots were generated using the EnhancedVolcano R package (version 3.17). qPCR validation of selected DEGs was performed as described in the Additional file 1: Supplementary Materials and Methods.

Proximity ligation assay

Proximity ligation assays (PLA) were performed using the NaveniFlexMR PLA kit (Navinci). Briefly, cells seeded in 8-well chamber slides were fixed with 4% formaldehyde for 15 min and permeabilized with 0.1% Triton-X in PBS for 10 min after 3 PBS washes. Afterwards, fixed

cells were washed with PBS thrice then incubated with blocking buffer at 37 °C for 1 h. Primary antibody incubation was then performed overnight at 4 °C using the appropriate antibody dilutions. The next day, cells were incubated with the anti-mouse and anti-rabbit Navenibodies (Navinci) at 37 °C for 1 h. Afterwards, the three enzymatic reactions were carried out following the manufacturer's protocol. After the third reaction, cells were washed in 1X TBS for 10 min twice, then finally washed in 0.1X TBS for 15 min. Slides were then dried, mounted with VectaShield® HardSet™ with DAPI, and covered with coverslips. Images were captured as specified above. For each field, PLA signals were measured and normalized to nuclei count using an in-house ImageJ script provided by the Light Microscopy Facility of the DKFZ.

Measurement of EGFR activation and degradation kinetics

A total of 2.0×10^5 GBM cells in 2 mL of DMEM maintenance medium were seeded into 35-mm cell culture dishes and were incubated at 37 °C, 5% CO₂ overnight. After overnight incubation, cells were serum-starved by replacing old medium with an equivalent volume of DMEM and 1% antibiotic–antimycotic. Serum-starved cells were incubated overnight. Cells were then treated with 100 µg/mL of the protein synthesis inhibitor cycloheximide (Sigma-Aldrich C4859) for 1 h. Afterwards, the old serum-free medium was replaced with new serum-free media with or without 100 ng/mL EGF (Peprotech AF-100-15). For each experimental condition (i.e., control and EMP3 KO), four dishes containing EGF-treated cells were incubated for 2 h, and lysates were collected at the following intervals: $t=30, 60, 90,$ and 120 min after EGF treatment. Untreated cells served as control and was considered as time point $t=0$. Lysates were stored in -80 °C until Western blot was performed.

Cell proliferation and apoptosis assays

Cell proliferation was measured using CellTiter-Glo 3D (Promega G9683) following the manufacturer's instructions. Caspase 3/7 activity was measured using the Caspase-Glo 3/7 Assay Kit (Promega G8091). Pre-treatment of cells with EGF, staurosporine, AZD9291, and K03861, as well as measurement of apoptotic activity via PARP cleavage, are further described in the Additional file 1: Supplementary Materials and Methods.

Statistical analyses

All other data apart from the LC–MS/MS data were statistically analyzed in GraphPad Prism version 9.3.1. Unpaired t-test was used when comparing two groups with equal variances. Welch's t-test was used when comparing two groups with unequal variances. Welch's ANOVA with Dunnett's T3 multiple comparisons test

was used when comparing more than two groups with unequal variances.

Results

Establishment of BioID2-based proximity labeling in GBM cells

To define EMP3's interactome, we performed BioID2-based proximity labeling [30] using U-118 GBM cells (Additional file 2: Fig. S1A–C). We stably transfected U-118 cells with pMXs plasmids encoding bait proteins tagged with a Myc-glycine-serine linker-BioID2 cassette at their C-terminal ends (Additional file 2: Fig. S1A). To determine if there are interactions that may be dependent on glycosylation, both wild-type (EMP3 WT) and the glycosylation-deficient N47A mutant forms of EMP3 (EMP3 N47A) were used as baits (Additional file 2: Fig. S1B). For spatial reference controls, TagRFP and a membrane-localizing form fused to an N-terminal GAP-43-derived membrane-targeting signal (GAP-TagRFP) were used. These controls were selected to identify both cytosolic and plasma membrane interactors of EMP3, since EMP3 resides in both compartments [13, 43, 58]. Immunofluorescence staining (Additional file 2: Fig. S2A–S2B) and Western blotting of the Myc tag (Additional file 2: Fig. S2C) confirmed proper subcellular localization and expression of the BioID2-tagged bait proteins. To prepare samples for mass spectrometry analysis, stably transfected cells were treated with 50 µM biotin for 18 h, and biotinylated proteins were purified by streptavidin pull-down (Additional file 2: Fig. S1C). Blotting of total lysates with streptavidin-HRP and Coomassie staining verified successful biotinylation and purification of biotinylated proteins, respectively (Additional file 2: Fig. S2C).

Mass spectrometry analysis of streptavidin pull-downs identified a total of 217 EMP3 WT-proximal proteins when TagRFP was used as the control, and 213 proteins when GAP-TagRFP was used (Fig. 1A). These included proteins that satisfied the filtering criteria (i.e., log₂-fold change (FC) vs. spatial reference control ≥ 1 ; Welch's t-test P -value ≤ 0.05), as well as proteins that were uniquely detected in the EMP3 WT pull-downs but were absent (i.e., label-free quantification or LFQ intensity = 0 in all three replicates) in either spatial reference control (Additional file 3). Previously known EMP3 interactors (e.g., CD44, CD47, FLOT1, VAMP3, and ATP5B) were identified using our filtering strategy, thus validating the selected log₂-FC and P -value cutoffs (Additional file 2: Fig. S3A, B). Notably, the choice of spatial reference control influenced which proteins were identified as potential EMP3 interactors. Hits that were selectively enriched in EMP3 WT relative to TagRFP cells (EMP3 WT/TagRFP) contained a greater proportion of plasma membrane-localized proteins (52.88% vs. 32.83% with

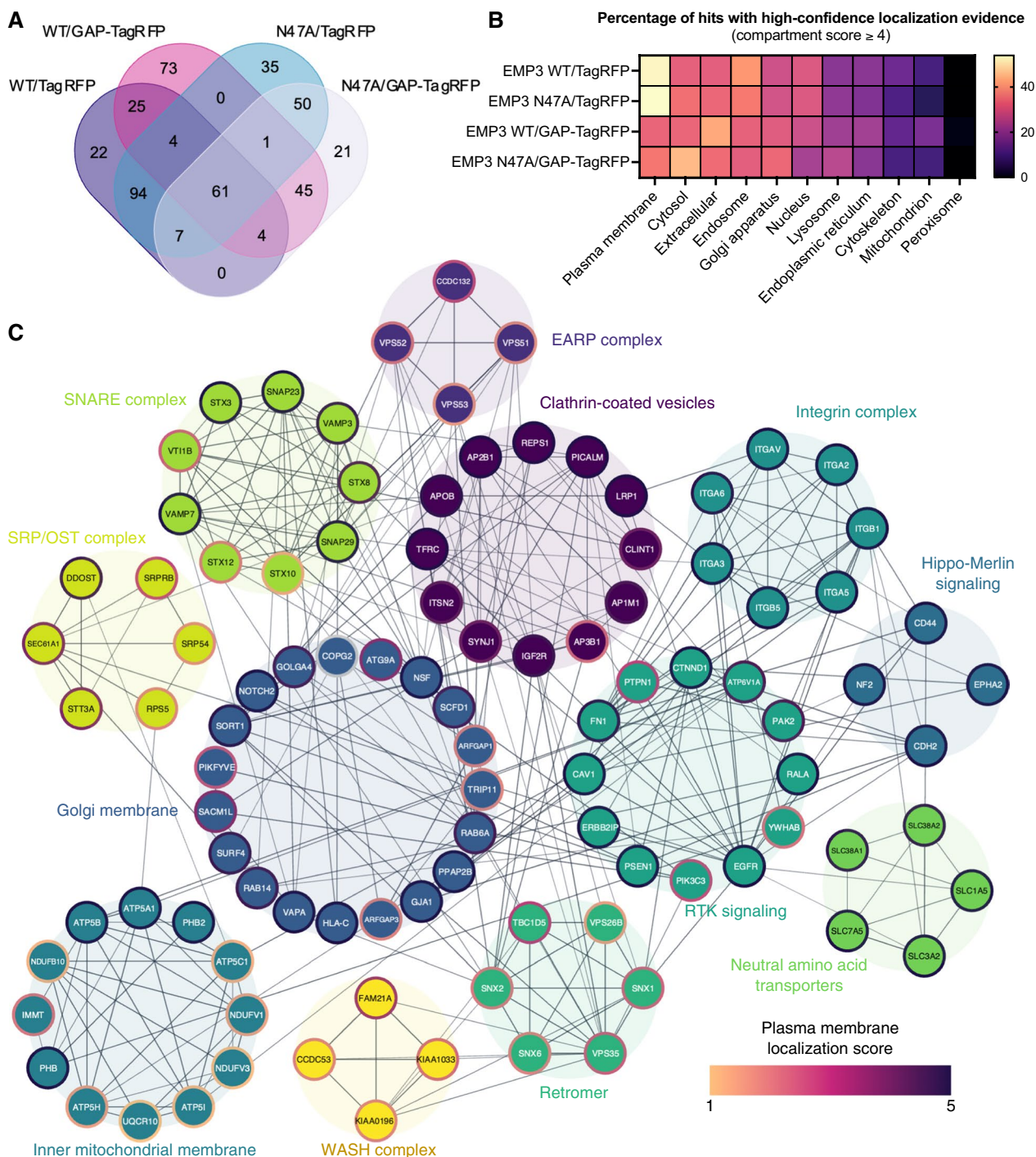


Fig. 1 BioID2-based proximity labeling of EMP3 WT and N47A in U-118 glioblastoma cells. **A** Venn diagram showing the number and extent of overlap of identified EMP3-proximal proteins between all pairwise comparisons. **B** Heat map showing the percentage of EMP3-proximal proteins with localization scores ≥ 4 in each cellular compartment and for each pairwise comparison. **C** STRING interaction network resulting from the union of hits identified with EMP3 WT as bait and TagRFP or GAP-TagRFP as spatial reference controls. Edges corresponding to STRING scores > 0.700 and nodes with degrees ≥ 3 were included in the network. Nodes were clustered into functional groups based on STRING enrichment analysis. For simplicity, nodes not belonging to any cluster were removed from the network. Node borders are colored according to plasma membrane localization score, while edge thickness corresponds to STRING interaction scores

GAP-TagRFP as the control) (Fig. 1B and Additional file 4). In contrast, EMP3 WT hits that were enriched relative to GAP-TagRFP (EMP3 WT/GAP-TagRFP) had a bias for cytosolic proteins (42.21% vs. 31.71% in EMP3 WT/TagRFP). Given EMP3's nature as a trafficking protein, the distinct interactors identified using either the TagRFP or GAP-TagRFP spatial reference control likely represent proteins that preferentially interact with membrane or cytosolic pools of EMP3, respectively. Thus, we took the total pool of EMP3 WT hits consisting of 336 proteins to comprise the full EMP3 interaction network.

BioID2-based proximity labeling identifies EGFR and endocytic trafficking regulators as EMP3 interactors

To provide a comprehensive spatial and functional picture of this interactome, network mapping was performed in STRING (version 11.5) using the union of EMP3/TagRFP and EMP3/GAP-TagRFP hits as input. Additional filtering for high-confidence interactions (STRING score ≥ 0.700) and well-connected nodes (degree ≥ 3) followed by enrichment analysis in Cytoscape (version 3.9.1) revealed an interaction network consisting of the GBM driver EGFR, as well as various spatial regulators of receptor trafficking (Fig. 1C). The latter included components of clathrin-coated vesicles (CCVs) as well as retromer, endosome-associated recycling protein (EARP), soluble

N-ethylmaleimide-sensitive fusion protein attachment protein receptors (SNARE), and Wiskott Aldrich Syndrome protein and scar homologue (WASH) complexes. Notably, all members of the retromer complex, several CCV-associated proteins (e.g., IGF2R, CLINT1, ITSN2, TFRC, and LRP1), SNARE proteins (e.g., VAMP3; VAMP2, VAMP7, STX12, VTI1B), and the extracellular matrix receptor CD44 were enriched regardless of which spatial reference control was used (Additional file 2: Fig. S3C). This suggests that these proteins may interact with both membrane or cytosolic pools of EMP3 or consistently co-traffic with EMP3 as it moves to and from both cellular compartments. Expectedly, most transmembrane proteins were preferentially enriched in the EMP3/TagRFP set and therefore were more likely to be proximal to membrane pools of EMP3. The EARP complex, which is involved in recycling internalized receptors back to the cell surface [51], was also selectively enriched in this set. Proximity ligation assay (PLA) in U-118 cells further validated EGFR, CLINT1, the EARP component VPS53, and several retromer proteins (TBC1D5, SNX1, SNX2) as EMP3 interactors (Fig. 2).

On the other hand, the cytosolic pool of EMP3 selectively interacted with proteins that facilitate targeting of nascent multi-pass membrane proteins towards the ER membrane (e.g., SRPRB, SRP54, SEC61A1). Cytosolic

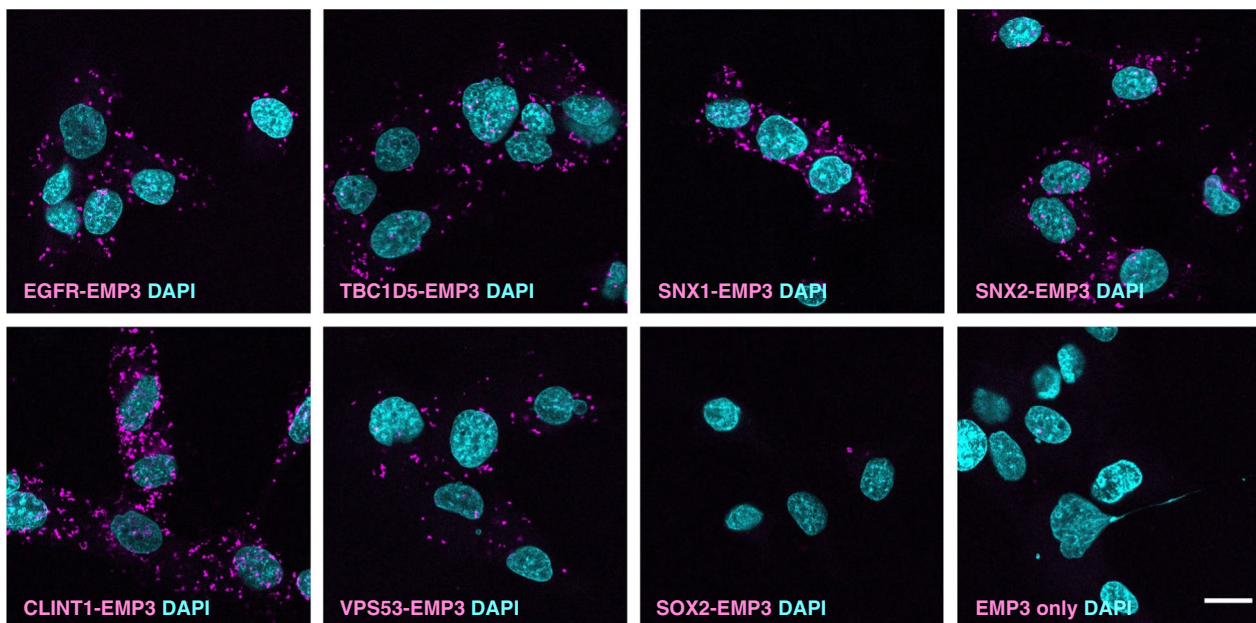


Fig. 2 Validation of selected BioID2-identified EMP3-proximal proteins using proximity ligation assay (PLA). PLA signals (magenta) indicating physical proximity (~ 40 nm) between EMP3 and various BioID2 hits, including EGFR, retromer components (TBC1D5, SNX1, SNX2), clathrin-coated vesicle-associated protein CLINT1 and EARP complex member VPS53. SOX2 was used as negative control. Nuclei are colored in cyan. Scale bar = 20 μ m

EMP3 was also selectively proximal to components of the oligosaccharyltransferase (OST) complex (e.g., STT3A, DDOST), which facilitate co-translational *N*-glycosylation of nascent proteins [22, 55]. Interestingly, the interaction with DDOST was lost when the EMP3 N47A mutant was used as bait, hinting that the asparagine residue at this position may mediate proper recognition of this OST subunit. We also observed several Golgi- and inner mitochondrial membrane-localizing hits that were not significantly enriched when EMP3 N47A was used as bait (Additional file 2: Fig. S3C), suggesting that glycosylated EMP3 may uniquely localize toward these compartments. Nonetheless, most membrane and trafficking proteins retained their enrichment even with the N47A mutation (Additional file 2: Fig. S3C). Collectively, these results indicate that while *N*-linked glycosylation may confer EMP3 with an organelle-specific function, it is not required for its membrane localization and interaction with most trafficking regulators.

EMP3 restricts EGF-induced late endosomal shuttling of EGFR and its eventual degradation in a TBC1D5-dependent manner

Given its association with membrane receptors and trafficking regulators, we then hypothesized that EMP3 may actively regulate certain receptor trafficking events. Thus, we focused our investigations on the possible effect of EMP3 on the intracellular trafficking of EGFR. To this end, we first generated and validated CRISPR/Cas9-edited EMP3 knockouts using U-118 and DK-MG GBM cells (Additional file 2: Fig. S4A–C). These cells exhibit the chromosome +7/–10 signature of GBM and express wild-type EGFR, making them a suitable model for investigating EGFR dynamics in GBM (Additional file 2: Fig. S4D, E and Additional file 5). Afterwards, we examined the kinetics of EGFR activation and degradation upon EGF treatment of control and EMP3 KO cells pre-treated with 100 µg/mL of the protein synthesis inhibitor cycloheximide for 1 h. Apart from inducing EGFR phosphorylation, EGF also stimulates the internalization and subsequent degradation of EGFR in lysosomes [2]. Consistent with this, Western blots showed continuous EGFR degradation in EGF-treated cells over the course of 2 h. Noticeably, ligand-induced degradation of total and phosphorylated EGFR (Tyr 1068) was accelerated in EMP3 KO cells (Fig. 3A and B), indicating that EMP3 limits EGF-induced endolysosomal degradation of EGFR. Given EMP3's interaction with several trafficking proteins, we then hypothesized that EMP3 may attenuate EGFR degradation specifically by restricting receptor trafficking towards degradative endosomes. Supporting this, we observed increased association of phosphorylated EGFR (Tyr1068) with the late endosomal marker

RAB7 in EMP3 KO cells 30 min after EGF treatment by PLA (Fig. 3C and D).

To elucidate the mechanism by which EMP3-dependent restriction of EGFR degradation could occur, we focused our attention on TBC1D5, a top interactor of cytosolic EMP3 (Additional file 2: Fig. S3B) and a retromer component that facilitates GTP hydrolysis and subsequent inactivation of RAB7 [28, 52, 53]. Loss of TBC1D5 function has been shown to convert RAB7 into a hyperactive, GTP-locked state [28]. Active RAB7, in turn, facilitates the fusion of late endosomes with lysosomes, leading to the degradation of late endosomal cargoes like EGFR [2, 4, 16, 25]. Given this information, we hypothesized that EMP3 and TBC1D5 may cooperate to restrict RAB7-mediated degradation of internalized EGFR. Indeed, overexpression of wild-type TBC1D5 (TBC1D5 WT), but not the GAP activity-deficient TBC1D5 R169A/Q204A mutant [21], reversed accelerated degradation of EGFR in EMP3 KO cells (Fig. 3E and F). Thus, EMP3 restricts EGFR degradation in a manner that is dependent on the RAB7 negative regulator TBC1D5.

Phosphoproteomic analysis reveals that EMP3 KO converges into CDK2 inhibition

To identify what signaling defects result from the loss of EMP3 and its EGFR-stabilizing effect, we performed mass spectrometry-based phosphoproteomic analysis of EMP3 KO and control cells cultured in normal maintenance medium for 72 h. On average, we detected a total of 8892 class I serine/threonine/tyrosine (STY) phosphosites (i.e., localization probability ≥ 0.75) across all samples, while an average of 4013 proteins were quantified in a full proteome analysis performed in parallel (Additional file 2: Fig. S5A, B). For downstream analysis, we only considered phosphosites that were detected in at least 2 out of 3 replicates per condition. Using this filter, we identified 1408 differentially phosphorylated proteins (i.e., proteins with phosphosite $|\log_2\text{-FC}|$ between EMP3 KO vs. control ≥ 1 ; FDR-adjusted P -value ≤ 0.05) in DK-MG cells (Additional file 6). In U-118 cells, there were 435 differentially phosphorylated proteins between EMP3 KOs and controls (Additional file 6). Majority of the differentially phosphorylated proteins were not differentially abundant at the full proteome level, indicating that most of the phosphorylation changes were driven by signaling alterations instead of changes in protein abundance. Moreover, both DK-MG and U-118 EMP3 KOs displayed higher percentages of class I phosphosite alterations than protein abundance changes (Additional file 2: Fig. S5C, D). This suggests that globally, EMP3 KO has a greater effect on protein activity than on protein levels. Notably, a higher proportion of DK-MG phosphosites exhibited significant

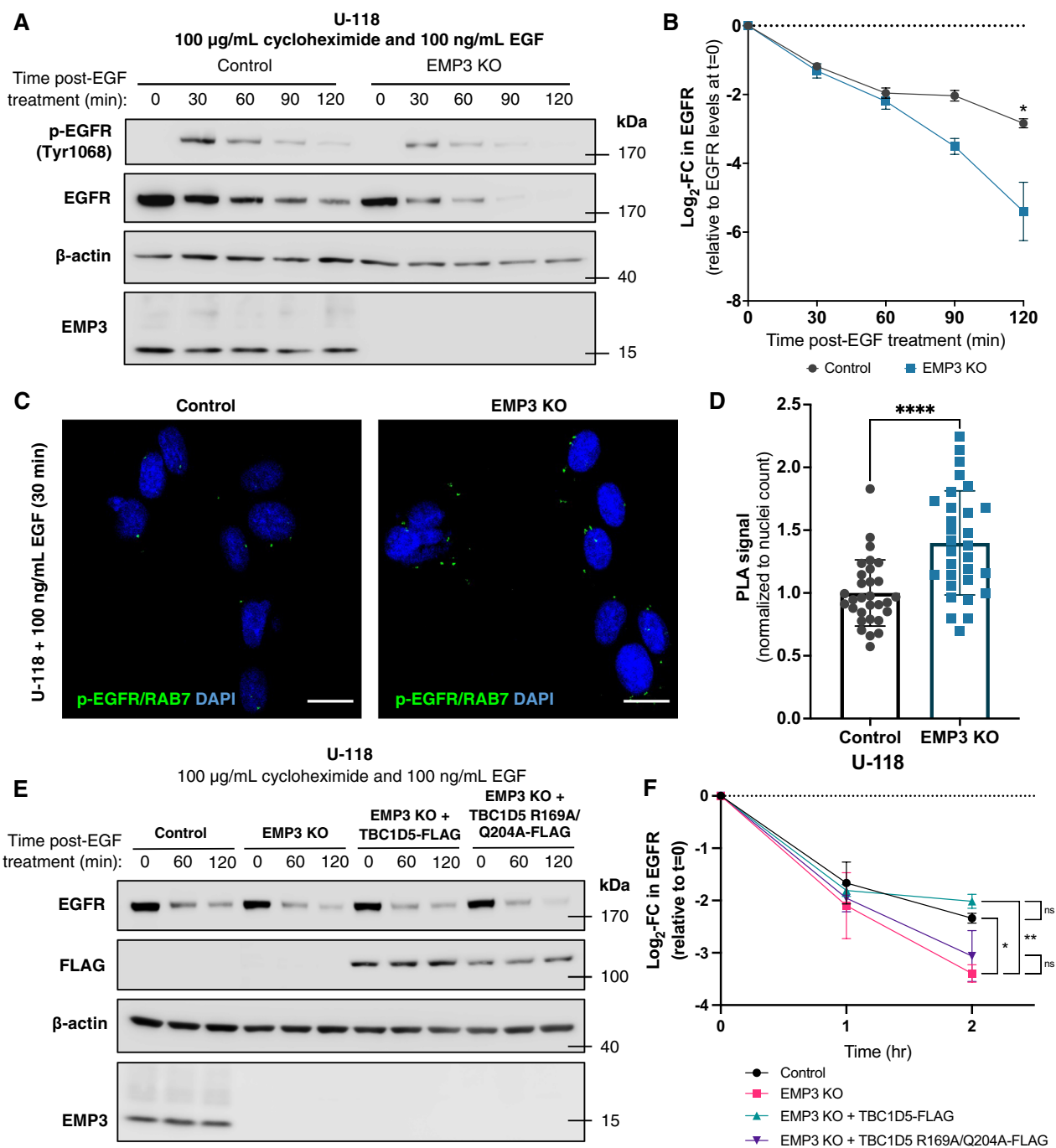


Fig. 3 EMP3 restricts RAB7 shuttling and ligand-induced degradation of EGFR in a TBC1D5-dependent manner. **A** Western blot showing the kinetics of EGFR phosphorylation (p-EGFR Tyr1068) and degradation (total EGFR) in U-118 control and EMP3 KO cells over the course of 2 h after treatment with 100 ng/mL EGF (n = 3). **B** Quantification of EGF-induced degradation of EGFR in U-118 control and EMP3 KO cells after treatment with 100 ng/mL EGF (n = 3). Band intensities of EGFR were normalized to β-actin, and log₂-fold changes (mean + S.E.M.) were calculated relative to the EGFR level at t = 0 and plotted over time. (Welch’s two-tailed t-test; *P < 0.05). **C** Representative PLA images testing the association between p-EGFR and RAB7 after 30-min EGF treatment of U-118 control and EMP3 KO cells (n = 3). **D** Quantification of p-EGFR-RAB7 PLA signals from EGF-treated U-118 control and EMP3 KO cells. PLA signals were derived from 30 random fields from n = 3 independent experiments (10 fields/experiment). Signals were normalized to nuclei count per field (Welch’s two-tailed t-test; ****P = < 0.0001). **E** Western blot showing TBC1D5 WT-mediated rescue of enhanced EGFR degradation in U-118 EMP3 KO cells (n = 3). **F** Quantification of EGF-induced EGFR degradation in U-118 control, EMP3 KO, EMP3 KO + TBC1D5 WT, and EMP3 KO + TBC1D5 R169A/Q204A (n = 3). Log₂-fold changes (mean + S.E.M.) were calculated and plotted as described (Welch’s ANOVA with Dunnett’s T3 multiple comparisons test; *P < 0.05)

log₂-FCs compared to U-118 phosphosites (33.02% vs. 6.98%), indicating that DK-MG is more susceptible to signaling alterations secondary to EMP3 KO (Additional file 2: Fig. S5C). Intersection of the phosphosites revealed a total of 197 STY residues undergoing phosphorylation changes (i.e., |log₂-FC| ≥ 1; FDR-adjusted *P*-value ≤ 0.05) in both DK-MG and U-118 EMP3 KOs (Fig. 4A). Strikingly, 82.23% of these 197 phosphosites were commonly dephosphorylated (i.e., log₂-FC ≤ -1 in both cell lines) upon EMP3 KO. In contrast, only 3.04% phosphosites were commonly phosphorylated (i.e., log₂-FC ≥ 1 in both cell lines), while 14.72% were differentially phosphorylated (i.e., log₂-FCs in the two cell lines going in opposite directions). Enrichment analysis revealed that the proteins with commonly dephosphorylated sites in the two EMP3 KO cell lines are mostly involved in the cell cycle (Fig. 4B). Thus, EMP3 KO results in the dephosphorylation of cell cycle regulators.

To identify upstream master regulators (MRs) that can explain these phosphoproteomic alterations, we performed phosphorylation analysis using Ingenuity Pathway Analysis (IPA, Qiagen). Intersection of the MRs revealed 4 common alterations in DK-MG and U-118 EMP3 KOs, including inhibition of the cyclin-dependent kinase CDK2 [33] and activation of CDKN1C, a negative regulator of cell proliferation [3] (Fig. 4C). In parallel, we also performed Kinase Enrichment Analysis (KEA) to predict upstream kinases that may be responsible for the observed phosphosite changes. KEA uses multiple kinase-substrate (KS) databases (i.e., KSIN, PhosD, PTMsigDB) to infer upstream kinase regulators from an input list of proteins [34]. Because KEA does not consider the extent of phosphorylation changes (i.e., log₂-FC values), we restricted our analysis to proteins with commonly dephosphorylated sites in DK-MG and U-118 EMP3 KOs, as dephosphorylated sites were overrepresented in our analysis. We

reasoned that inhibition of certain upstream kinases may account for the high prevalence of these dephosphorylated proteins. KEA consistently predicted CDK2 to be an upstream kinase regulator affected by EMP3 KO across all three KS databases (Fig. 4D). Thus, inhibition of CDK2 activity may largely explain the dephosphorylation of the input substrates in EMP3 KO cells.

One potential limitation of IPA and KEA is that the amino acid identities of the differentially phosphorylated residues are not accounted for in the pathway analysis. To identify upstream kinases based on the phosphosite alterations induced by EMP3 KO, we performed Robust Inference of Kinase Activity or RoKAI [65]. For this analysis, we used commonly regulated STY sites (i.e., FDR-adjusted *P*-value ≤ 0.05, log₂-FC ≥ 1 or ≤ -1 and going in the same direction in both EMP3 KO cell lines) and their corresponding phosphorylation log₂-FCs upon EMP3 KO as input. In agreement with the IPA and KEA analyses, RoKAI also indicated significant inhibition of CDK2 based on the phosphorylation changes that occurred in both cell lines (Fig. 4E). To validate our bioinformatic analyses, we assessed and compared the protein levels of CDK2 in control and EMP3 KO cells by Western blotting. Results confirmed that total CDK2 levels are significantly reduced in EMP3 KO cells (Fig. 4F–G). In summary, integration of the three phosphoproteomic analysis pipelines reveals that EMP3 KO converges into CDK2 inhibition and the dephosphorylation of CDK2 substrates involved in cell cycle progression.

Loss of EMP3 inhibits EGFR-dependent and cell cycle-related transcriptional programs

Next, we sought to determine how loss of EMP3 impacts transcriptional programs. To this end, we performed microarray analysis on total RNA extracted from 72-h cultures of U-118 and DK-MG cells with or without EMP3. A total of 1183 and 1452 differentially expressed

(See figure on next page.)

Fig. 4 Phosphoproteomic analysis of proteins with commonly regulated phosphosites in DK-MG and U-118 EMP3 KOs. **A** Donut chart showing the distribution of phosphorylation changes common to both DK-MG and U-118 EMP3 KO cells relative to their respective controls. Commonly phosphorylated—log₂-FC ≥ 1, FDR *P*-value ≤ 0.05 in both DK-MG and U-118; Commonly dephosphorylated—log₂-FC ≤ -1, FDR *P*-value ≤ 0.05 in both DK-MG and U-118; Differentially phosphorylated—FDR *P*-value ≤ 0.05 but log₂-FC in opposite directions in DK-MG and U-118. **B** Reactome pathways enriched based on proteins with phosphosites that are dephosphorylated in both DK-MG and U-118 EMP3 KOs. Circle sizes correspond to the number of proteins associated with each term, while the color scale indicates the significance level. **C** Heatmap showing IPA MRs that are activated or inhibited (|activation z-score| ≥ 2, *P*-value ≤ 0.05) in both DK-MG and U-118 EMP3 KOs and their respective activation z-scores, colored according to predicted activity (red—active; blue—inactive). **D** KEA of proteins with commonly dephosphorylated sites in both DK-MG and U-118 EMP3 KOs. From each kinase-substrate database, the top 5 kinases that phosphorylate substrates in the input list were identified and listed on the y-axis. Circle sizes depict substrate number, while the color scale indicates the significance level of each kinase. **E** RoKAI of proteins with commonly regulated sites in DK-MG (left) and U-118 EMP3 KOs (right). Upstream kinases are listed on the y-axis and ordered according to significance level. Those with -log₁₀(FDR-adjusted *P*-values) = ∞ were arbitrarily scored as 15 on the x-axis to allow plotting. Circle sizes indicate substrate number, while the color scale shows predicted kinase activity (red—active; blue—inactive). **F** Western blots of CDK2 in control and EMP3 KO cells. **G** Quantification of CDK2 band intensities (mean + S.D.) normalized to β-actin and calibrated relative to control cells (n = 3; Welch's two-tailed t-test; **P* < 0.05; ***P* < 0.01)

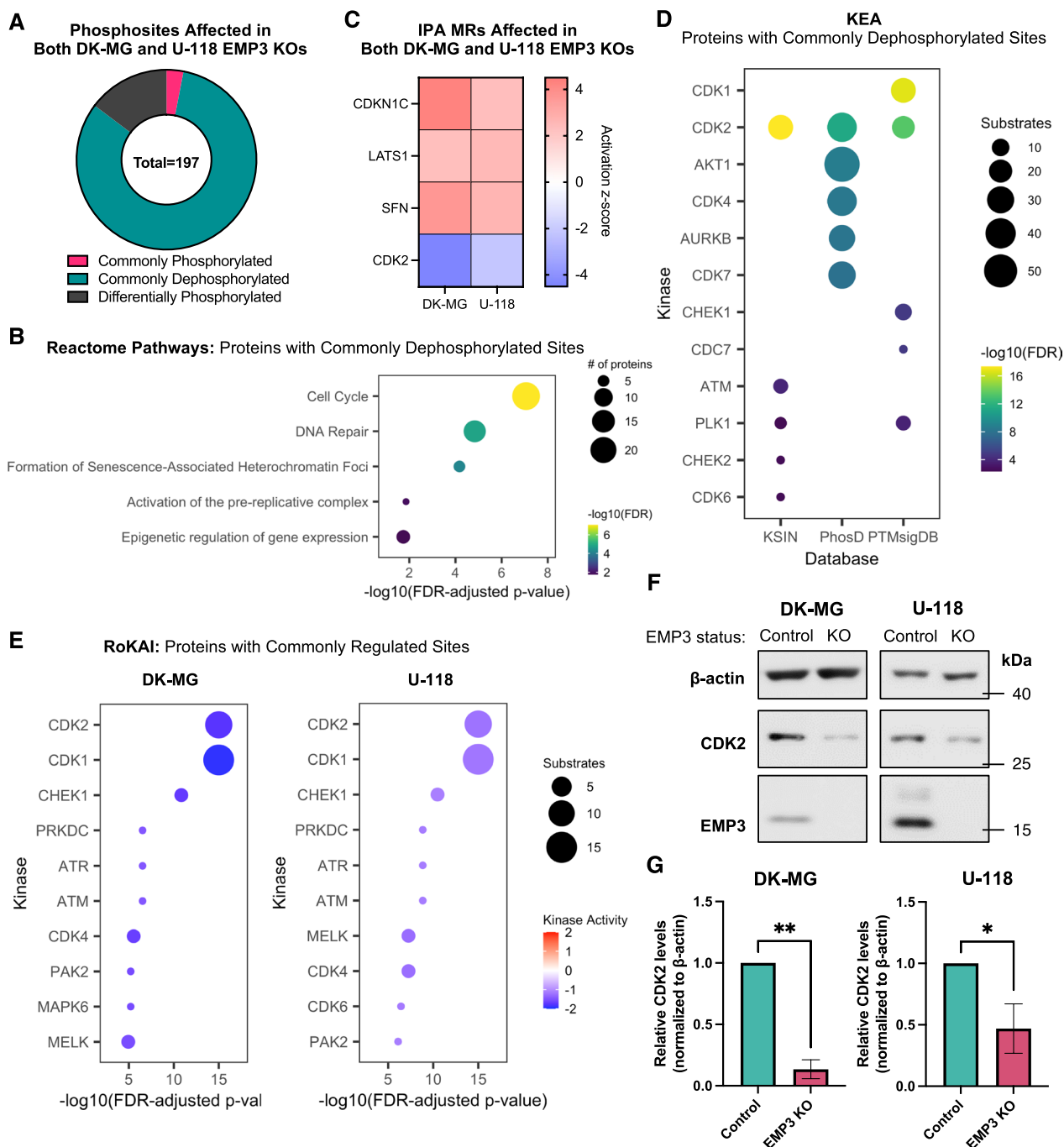


Fig. 4 (See legend on previous page.)

genes (DEGs) were identified upon EMP3 depletion in U-118 and DK-MG cells, respectively (Additional file 7). Among these, 645 upregulated and 538 downregulated genes were identified in U-118 EMP3 KO cells, while 636 upregulated and 816 downregulated genes were identified in DK-MG EMP3 KOs. We then performed pathway analyses to identify what transcriptional programs

are enriched based on our DEG lists (Fig. 5A–D). KEGG pathway analysis did not reveal any enriched pathways when using the set of genes that were upregulated in both EMP3 KO cell lines. However, consistent with CDK2 inhibition, we identified 128 DNA replication- and cell cycle-related genes that are downregulated in both DK-MG and U-118 EMP3 KOs (Fig. 5A and C).

We also used the DEGs from each cell line as input for IPA to predict which upstream signaling pathways are differentially regulated between control and EMP3 KO conditions. This analysis yielded a total of 43 MRs that were inhibited in both DK-MG and U-118 EMP3 KO cells (Fig. 5B). Consistent with impaired EGFR function, EGF was identified to be among the most significantly inhibited MRs in both U-118 (activation z-score = -2.635, $P = 2.43 \times 10^{-32}$) and DK-MG (activation z-score = -2.92, $P = 1.10 \times 10^{-17}$) EMP3 KO cells (Additional file 2: Fig. S6A, B). KEGG pathway analysis of the 43 commonly inhibited MRs further indicated enrichment of proteins involved in EGFR tyrosine kinase inhibitor resistance, hinting that the therapeutic response of GBM cells against EGFR-targeting compounds may be attenuated in the absence of EMP3 (Fig. 5D). In line with this, gene set enrichment analyses (GSEA) of the U-118 and DK-MG DEGs also revealed upregulation of the “KOBAYASHI_EGFR_SIGNALING_24HR_DN” gene set in EMP3-expressing control cells (Fig. 5E and Additional file 2: Fig. S6C). This gene signature includes genes that are downregulated upon EGFR inhibition of non-small cell lung cancer (NSCLC) cells [32]; thus, EMP3 control cells can be presumed to have an intact EGFR function, as these cells retain the expression of genes that are negatively affected by EGFR inhibition. Conversely, U-118 and DK-MG EMP3 KO cells exhibited increased expression of genes that are upregulated upon EGFR inhibition of NSCLC cells (Fig. 5F and Additional file 2: Fig. S6D). To further validate these transcriptomic results, we selected 4 of the top 5 DEGs (*ORC6*, *RFC2*, *CDC6*, *MCM7*) that are EGF/EGFR targets according to our IPA and GSEA analyses and are involved in DNA replication or the cell cycle according to KEGG. qPCR analysis confirmed that these 4 genes are downregulated in U-118 and DK-MG EMP3 KOs relative to controls (Fig. 5G and Additional file 2: Fig. S6E, respectively). Taken together, multiple gene enrichment and pathway analyses indicate that EMP3 KO represses the transcription of EGFR-dependent cell cycle genes.

EMP3 KO reduces mitogenic response to EGF and sensitizes GBM cells to EGFR inhibition

Our functional, phosphoproteomic, and transcriptomic data collectively indicate that targeting EMP3 inhibits EGFR/CDK2 signaling by reducing EGFR stability. To evaluate the phenotypic consequences of this process, we assessed how EMP3 KO impacts the proliferative capacity and response of GBM cells to ligand-dependent EGFR activation. Proliferation rates of EMP3 KO and control cells grown in serum-containing medium were measured for 96 h. Results consistently showed that in both cell lines, EMP3 KOs were less proliferative than controls (Fig. 6A and B). This is consistent with our phosphoproteomics and gene expression data indicating dysregulation of DNA replication and cell cycle progression in EMP3 KOs (Figs. 4B and 5C). To examine the effect of EMP3 on EGFR-dependent proliferation, we serum-starved EMP3 KO and control cells overnight and monitored their proliferation after daily treatment with 100 ng/mL EGF for 72 h. Serum starvation is presumed to eliminate external sources of mitogenic stimulation; thus, any changes in cell number over this period can be mainly attributed to the externally administered ligand. Consistent with attenuated EGFR signaling, U-118 and DK-MG EMP3 KO cells were less responsive to mitogenic stimulation by EGF (Fig. 6C and D).

Our -omics data indicated that several pathways and kinases related to EGFR signaling and tyrosine kinase inhibitor resistance are inhibited upon EMP3 depletion. To test whether this translates to increased sensitivity to kinase inhibition, we measured apoptotic rates in EMP3 KO and control cells upon pan-kinase inhibition with staurosporine (STS). STS is a broad-spectrum kinase inhibitor that binds to most kinases at submicromolar affinity [17]. Supporting our hypothesis, we observed that EMP3 depletion sensitizes U-118 and DK-MG cells to STS-induced apoptosis, as measured by higher caspase 3/7 activity (Fig. 6E and F) and greater cleaved PARP levels (Fig. 6G) in EMP3 KO cells. Thus, EMP3 may support the pro-survival activity of EGFR-dependent kinases, thereby allowing GBM cells to evade apoptotic cell death.

To further demonstrate the potential therapeutic relevance of EMP3 depletion, we also investigated whether

(See figure on next page.)

Fig. 5 Pathway analysis of differentially expressed genes between control and EMP3 KO cells. **A, B** Venn diagram showing the overlap of **(A)** downregulated genes ($\log_2\text{-FC} \leq -1$, FDR P -value ≤ 0.05) and **(B)** inhibited master regulators (activation z-score ≤ -2 , P -value ≤ 0.05) between DK-MG and U-118 EMP3 KOs. **C, D** KEGG pathways enriched based on the list of **(C)** commonly downregulated genes and **(D)** commonly inhibited MRs. **E, F** GSEA results showing upregulation of the gene sets KOBAYASHI_EGFR_SIGNALING_24HR_DN **(E)** and _UP **(F)** in U-118 control and EMP3 KO cells, respectively. Genes were sorted from left to right based on the difference of the \log_2 expression levels between control and EMP3 KO cells. Vertical black bars indicate the location of the genes contributing to the enrichment scores (ES). The ES, which indicate upregulation ($\text{ES} > 0$) or downregulation ($\text{ES} < 0$) of a certain gene, are plotted on the y-axis. NES: normalized enrichment score. **G** qPCR results validating the downregulation of selected genes in U-118 EMP3 KOs (unpaired one-tailed t-test; * $P = < 0.05$; ** $P = < 0.01$)

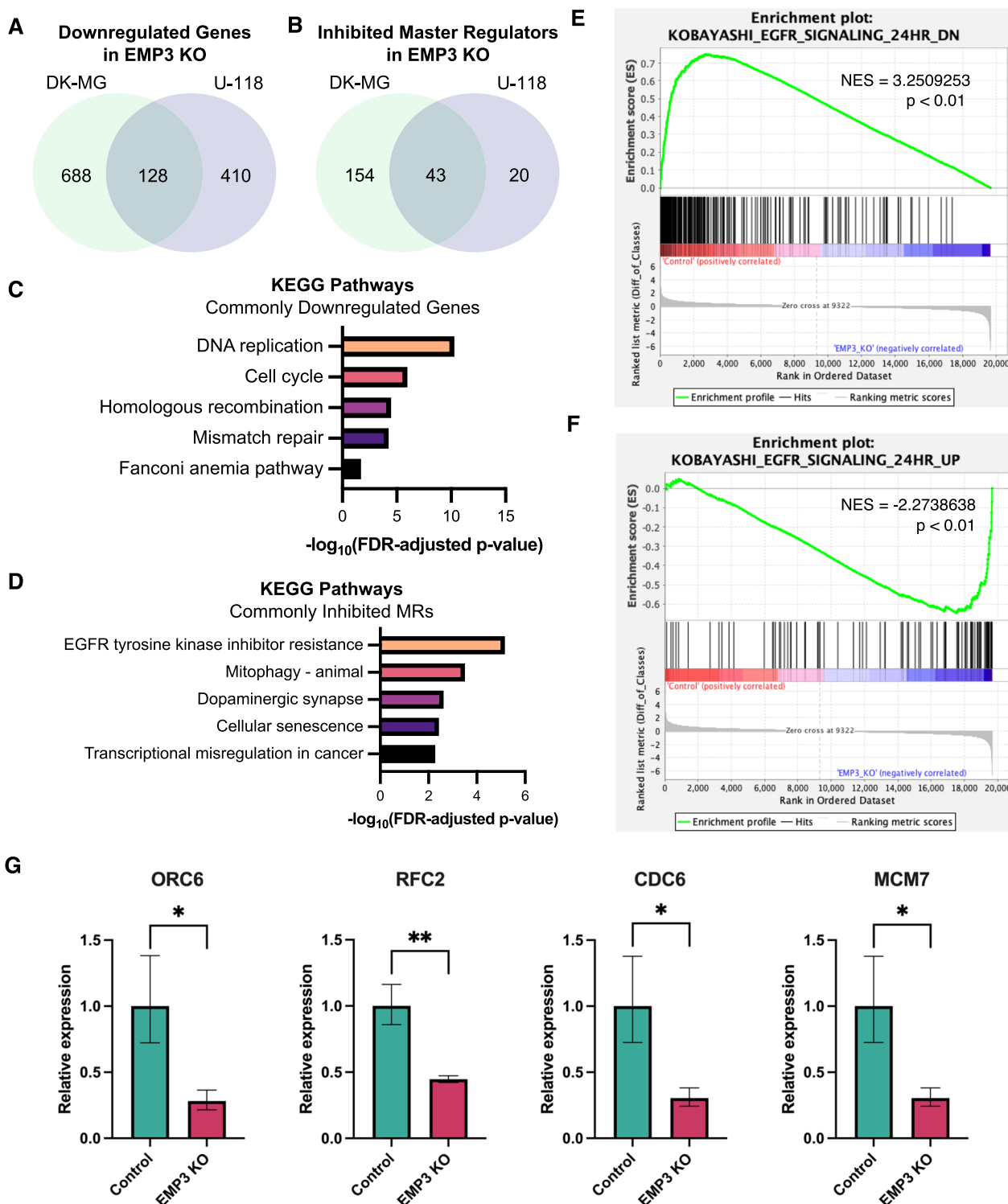


Fig. 5 (See legend on previous page.)

EMP3 KO and targeted EGFR inhibition can have a synergistic effect in GBM. To test this, we measured cell viability and active caspase 3/7 levels in U-118 cells after treatment with AZD9291 (osimertinib). AZD9291 is a

third-generation EGFR inhibitor that has shown efficacy against non-small-cell lung cancer [26]. Because it is highly brain-penetrant and can irreversibly inhibit both wild-type and mutant forms of EGFR, AZD9291

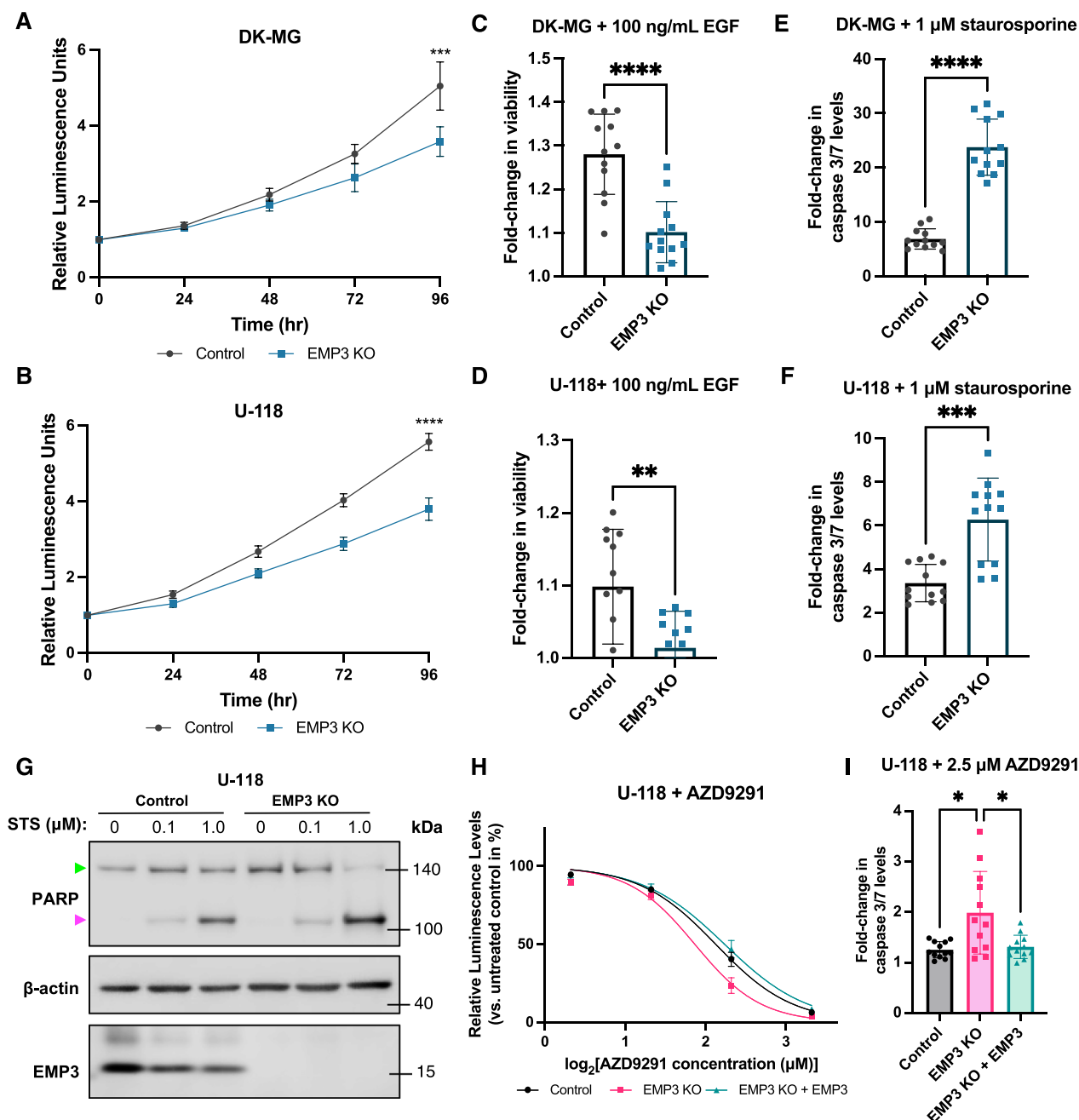


Fig. 6 EMP3 KO cells have impaired proliferative response and increased sensitivity to kinase inhibition. **A, B** Proliferation of DK-MG (**A**) and U-118 (**B**) control and EMP3 KO cells cultured in normal serum-containing medium over the course of 4 days. Dots represent mean fold-changes in CellTiter-Glo luminescence readings relative to $t=0$, while error bars show 95% confidence intervals (unpaired t-test; *** $P < 0.001$, **** $P < 0.0001$). **C, D** Proliferative response of serum-starved DK-MG (**C**) and U-118 (**D**) control and EMP3 KO cells to daily EGF treatment for 72 h. Bar plots represented mean fold-changes in CellTiter-Glo luminescence readings of EGF-treated cells versus untreated controls. Error bars and dots represent S.D. and individual measurements, respectively (unpaired t-test; ** $P < 0.01$, **** $P < 0.0001$). **E, F** Caspase 3/7 levels in DK-MG (**E**) and U-118 (**F**) control and EMP3 KO cells treated with 1 μM staurosporine (STS) for 4 h. Bar plots represent mean fold-changes in Caspase 3/7 luminescence readings of STS-treated cells versus untreated controls. Error bars and dots represent S.D. and individual measurements, respectively (Welch's t-test; *** $P < 0.001$, **** $P < 0.0001$). **G** Western blot showing full-length (green arrow) and cleaved PARP (magenta arrow) in U-118 control and EMP3 KO cells treated with 100 nM or 1 μM STS for 4 h. **H** Concentration–response curve of U-118 control, EMP3 KO, and EMP3 KO + EMP3 cells treated with the EGFR inhibitor AZD9291 for 24 h. Points represent mean percentage changes in CellTiter-Glo luminescence levels of treated cells relative to untreated cells, while error bars represent S.D. ($n = 3$). **I** Caspase 3/7 levels in U-118 control, EMP3 KO, and EMP3 KO + EMP3 cells treated with 2.5 μM AZD9291 for 24 h. Bars represent mean fold-changes in Caspase 3/7 luminescence readings of treated cells versus untreated controls. Error bars and dots represent S.D. and individual measurements, respectively (Welch's ANOVA with Dunn's T3 multiple comparisons test; * $P < 0.05$).

has been explored as a potential drug treatment for GBM [7, 10, 39]. Treatment of U-118 cells with AZD9291 for 24 h reduced cell viability in a dose-dependent manner (Fig. 6H). The concentration–response curve exhibited a statistically significant leftward shift upon EMP3 depletion, indicating a synergistic effect between EMP3 KO and EGFR-specific inhibition. This effect was reversed when EMP3 was re-expressed in EMP3 KO cells (Fig. 6H and Additional file 2: Fig. S7A), demonstrating that increased sensitivity to AZD9291 is a specific effect of EMP3 depletion. This effect was also reflected in the half-maximal inhibitory concentration (IC_{50}) values, which was significantly lower in EMP3 KO cells ($IC_{50}=3.65\ \mu\text{M}$) compared to control ($IC_{50}=4.37\ \mu\text{M}$) and EMP3 KO cells with the rescue construct ($IC_{50}=4.72\ \mu\text{M}$). Treatment with a sub- IC_{50} concentration of $2.5\ \mu\text{M}$ AZD9291 for 24 h also induced higher caspase 3/7 activity in EMP3 KO cells compared to control or EMP3 KOs with the rescue construct (Fig. 6I). Therefore, EMP3 contributes to therapeutic resistance against EGFR inhibition; conversely, targeting EMP3 may improve the effect of targeted EGFR inhibitors against GBM cells.

EMP3 silencing in EGFR-high patient-derived glioblastoma stem cells increases susceptibility to CDK2 inhibition

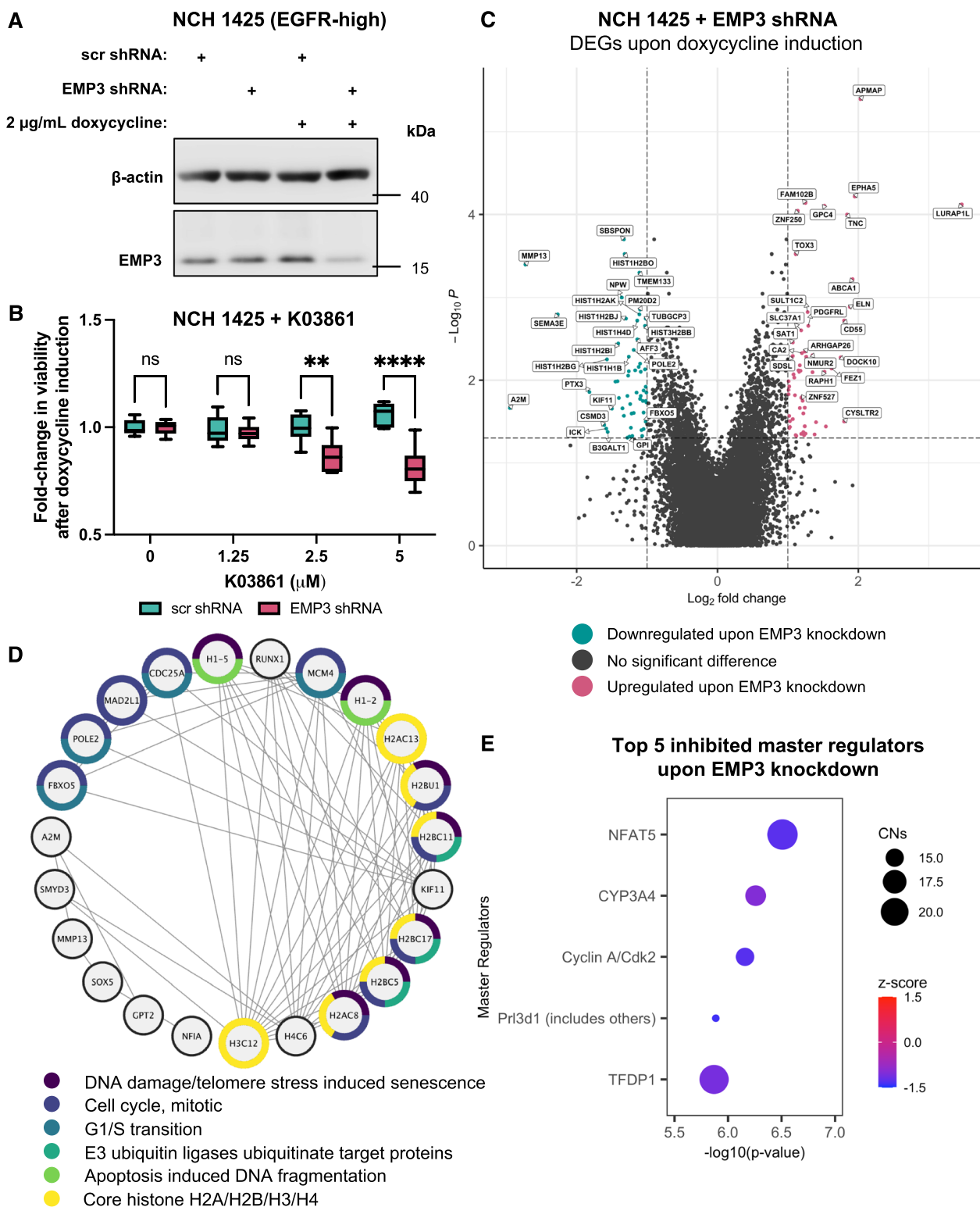
GBMs are known to harbor both differentiated and stem like-cells [15, 61]. Our DK-MG and U-118 cultures closely mimic differentiated GBM cells, as these cell lines are grown in differentiation-promoting, serum-containing medium and exhibit morphological features akin to astrocytes. To further test whether our findings are applicable to stem-like GBM cells, we also generated patient-derived glioblastoma stem cell (GSC) models cultured as three-dimensional (3D) spheroids in serum-free stem cell conditions. We obtained EGFR-high (NCH1425) and EGFR-low (NCH644) GSCs, as confirmed by Western blot and chromosomal copy number analysis (Additional file 2: Fig. S7B–D). These GSCs were additionally confirmed to express wild-type EGFR by whole exome sequencing (Additional file 5). Both GSCs were lentivirally transduced with doxycycline-inducible

non-targeting (scrambled) and EMP3-targeting short hairpin RNAs (shRNAs). Western blots confirm efficient knockdown of EMP3 in doxycycline-treated NCH1425 and NCH644 cells transduced with EMP3 shRNAs (Fig. 7A and Additional file 2: Fig. S8A). We then proceeded to test whether loss of EMP3 synergizes with CDK2 inhibition in an EGFR-dependent manner. We hypothesized that if EMP3 facilitates CDK2 activity primarily through EGFR, then EMP3 knockdown should synergize with CDK2 inhibition only in EGFR-high GSCs. Conversely, EGFR-low GSCs expressing EMP3 shRNAs should not exhibit increased susceptibility to CDK2 inhibition, because the EMP3/EGFR/CDK2 signaling axis is non-existent in this context. Indeed, treatment with the selective CDK2 inhibitor K03861 synergized with EMP3 knockdown in a dose-dependent manner in NCH1425 (Fig. 7B), but not in NCH644 GSCs (Additional file 2: Fig. S8B). Thus, like in differentiated GBM cells, EMP3 also facilitates CDK2 activity in an EGFR-dependent manner in stem-like GSCs.

To further correlate the increased K03861 vulnerability of EMP3-depleted NCH1425 GSCs with signaling defects, we performed microarray-based transcriptomic analysis of control and doxycycline-induced NCH1425 cells harboring either the scrambled or EMP3 shRNA. A total of 115 DEGs were identified upon doxycycline induction of EMP3 shRNA expression (Fig. 7C). Additional filtering revealed that only 85 of these DEGs were unique to NCH1425 cells expressing the EMP3 shRNA, while the other 30 genes were also differentially expressed in upon induction of scrambled shRNA and were therefore not considered in the subsequent analysis. (Additional file 2: Fig. S9A and Additional file 8). Out of the 85 genes uniquely affected by EMP3 silencing, 46 were downregulated and 39 were upregulated (Additional file 2: Fig. S9B). Consistent with impaired CDK2 activity, pathway analysis indicated that the downregulated genes are part of a functional gene expression network involved in DNA damage, cell cycle, and G1/S transition (Fig. 7D). Replication-dependent core histone genes (e.g., *H2AC13*,

(See figure on next page.)

Fig. 7 EMP3 silencing synergizes with CDK2 inhibition in EGFR-amplified NCH1425 GSCs. **A** Western blots verifying successful EMP3 silencing in doxycycline-treated NCH1425 GSCs transduced with inducible EMP3 shRNAs. **B** Fold-change in the viability of NCH1425 GSCs after induction of shRNA expression and treatment with increasing concentrations of the CDK2 inhibitor K03861 (multiple Welch's t-test; *** $P < 0.01$, **** $P < 0.0001$). **C** Volcano plots showing differentially expressed genes upon doxycycline-induction of EMP3 shRNA expression in NCH1425 cells. Genes that were upregulated and downregulated upon EMP3 silencing are colored red and green, respectively. **D** STRING network of downregulated genes in NCH1425 expressing the EMP3 shRNA. For simplicity, nodes not belonging to the main cluster were removed from the network. Node borders are colored according to Reactome and Pfam protein domain terms. **E** Top 5 inhibited MRs based on the 85 DEGs unique to NCH1425 expressing the EMP3 shRNA. MRs putatively regulating the input genes are listed on the y-axis and ordered according to significance. Circle sizes represent the number of associated causal networks (CNs) per MR, while the color scale indicates the activation z-score of each MR (red—active; blue—inactive)



H2BU1, H2BC11, H2BC17, H2BC5, H2AC8, H3C12), which are known to be downstream CDK2 targets [41, 67], were also overrepresented in the set of downregulated genes (Fig. 7D). Upstream pathway analysis of the 85 DEGs using IPA further identified cyclin A/CDK2 to be among the top 5 inhibited master regulators in EMP3-depleted NCH1425 cells. Taken together, these findings suggest that the increased susceptibility of EMP3-silenced NCH1425 cells to K03861 is due to their low baseline CDK2 activity, as measured by reduced transcription of CDK2-dependent cell cycle-related genes.

EMP3-high GBMs have elevated levels of total and phosphorylated EGFR

Lastly, to see whether our in vitro findings correspond to what is observed in actual tumor samples, we mined the TCGA GBM dataset using the Gliovis portal [5]. We searched for proteins upregulated in EMP3-high versus EMP3-low tumors (i.e., difference in reverse phase protein array (RPPA) scores >0; $P \leq 0.05$). Interestingly, both total and phosphorylated EGFR (Tyr1068 and Tyr1173) were among the top proteins with increased abundance in EMP3-high tumors (Fig. 8A). Other RTKs

(e.g., HER2) and BioID2-identified EMP3 interactors (e.g., TFRC, CAV1) also had higher protein abundances in EMP3-high tumors, hinting at possible EMP3-dependent regulation of these proteins as well. The higher levels of Tyr1068-phosphorylated (Fig. 8B) and total EGFR (Fig. 8C) in EMP3-high IDH-wt GBMs are consistent with our in vitro findings demonstrating increased degradation of EGFR upon EMP3 depletion. However, we did not observe the same positive correlation between EMP3 expression and CDK2 protein levels, and this may be due to the confounding effect of other upstream regulators of CDK2 activity in bulk tumor samples. Alternatively, changes in CDK2 levels may be very transient and/or restricted to a small population of actively dividing tumor cells and thus difficult to capture. Nonetheless, EMP3-dependent maintenance of EGFR stability and activity is consistent across biochemical, transcriptomic, phosphoproteomic, and phenotypic levels and can be further correlated with clinical data from the TCGA.

Discussion

In this study, we integrated protein–protein interaction (PPI) mapping with phosphoproteomics, transcriptomics, and functional characterization of CRISPR/

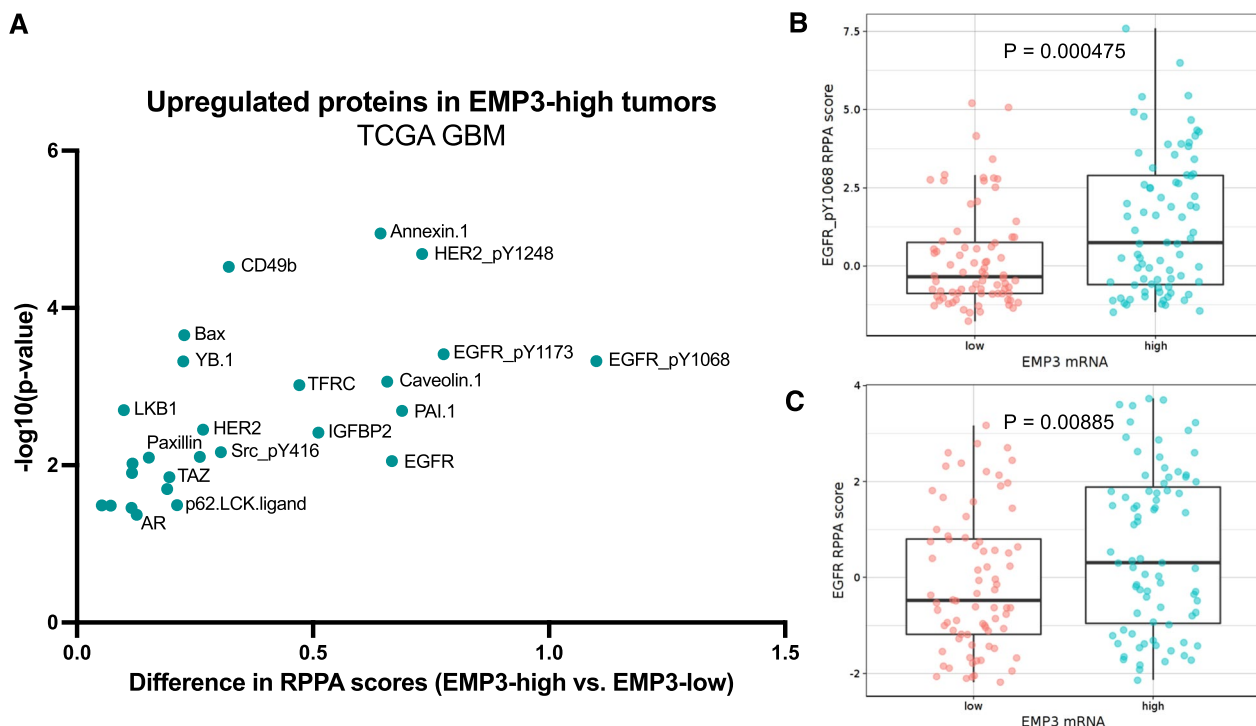


Fig. 8 Validation of EMP3's effects on total and phosphorylated EGFR using TCGA data. **A** Scatter plot showing upregulated proteins (difference in RPPA scores >0; $P < 0.05$) in EMP3-high vs. EMP3-low TCGA IDH-wt GBM tumors. Tumors were classified into either group using the median EMP3 expression level based on the TCGA Agilent-4502A microarray data as cutoff. **B, C** Representative bar plots showing the RPPA scores of Tyr1068-phosphorylated (**B**) and total EGFR (**C**) in EMP3-high vs. EMP3-low IDH-wt GBMs. Figures were obtained from the Gliovis portal version 0.20 (<http://gliovis.bioinfo.cnio.es/>, accessed 09 July 2022)

Cas9 KO cells to examine the molecular function of EMP3 in IDH-wt GBM. Our results show that EMP3 stabilizes EGFR, a frequently overactivated oncogene in IDH-wt GBM. Consistent with previous studies that showed inhibition of RTK signaling in non-glioma cells upon EMP3 silencing [13, 23, 63], we observed higher EGF-induced EGFR degradation in our EMP3 KO cells. Building on these findings, we further elucidated a novel link between the stabilization of EGFR and EMP3's trafficking function. Specifically, we have shown that EMP3 restricts EGFR trafficking into degradative endosomes, as loss of EMP3 promoted the association between ligand-activated EGFR and the late endosomal marker RAB7. These *in vitro* findings are consistent with TCGA data, which show reduced levels of both total and phosphorylated EGFR in GBMs with low EMP3 expression. In our experimental model, increased EGFR degradation was rescued by overexpression of the retromer component TBC1D5, a novel EMP3 interactor identified by our BioID2 screen. Other retromer components, including the sorting nexins SNX1 and SNX2, have been previously linked to the regulation of EGFR trafficking and stability [19, 36, 68]; however, to our knowledge, this is the first report of TBC1D5's involvement in regulating EGFR dynamics. As a RAB7 GTPase-activating protein (GAP), TBC1D5 inhibits several RAB7-mediated processes, including RAB7 localization to late endosomes [28, 37, 52, 53]. Critically, RAB7 mediates EGFR shuttling from late endosomes to lysosomes, thereby facilitating receptor degradation [2, 16]. Given these past findings and our present results, we propose that EMP3 facilitates TBC1D5 recruitment into maturing endosomes, where the latter could inactivate RAB7 and thus restrict the progression of internalized EGFR cargoes towards lysosomal degradation (Fig. 9). This model is consistent with previous work demonstrating TBC1D5-mediated retrieval of other receptors ITGA5, ITGB1, and IGF2R away from endolysosomal degradation [27]. Interestingly, we also identified these receptors as EMP3 interactors in our BioID2 screen, indicating that the EMP3-TBC1D5 complex may stabilize a broader set of GBM receptors beyond EGFR. Additional work will be necessary to systematically identify what other receptors are regulated by the EMP3-TBC1D5 interaction.

In addition to these mechanistic findings, our study also demonstrates how impaired EGFR trafficking and reduced EGFR stability upon EMP3 KO inhibit downstream oncogenic signaling. First, our phosphoproteomic data indicates that EMP3 KO leads to the inactivation of the cyclin-dependent kinase CDK2. CDK2, which is often upregulated in GBMs compared to normal brain tissue [38], has been shown to be downstream EGFR target in glioblastoma cell lines [8]. Its transient activation

by AKT is known to be a critical step in the induction of cell cycle progression [42]. Active CDK2, in turn, hyperphosphorylates retinoblastoma (RB1), thereby triggering the activation of E2F transcription factors and cell cycle progression [1, 11]. Apart from promoting *in vitro* proliferation of GBM cells, CDK2 also facilitates *in vivo* tumor growth as well as resistance to apoptosis induced by radiotherapy [62]. Consistent with concomitant EGFR and CDK2 inhibition, our gene expression data for differentiated GBM cells demonstrate that EMP3 KO leads to the downregulation of EGFR-responsive genes that are involved in DNA replication and cell cycle regulation. Additionally, loss of EMP3 impairs the transcription of EGF/EGFR-dependent genes that mediate tyrosine kinase inhibitor resistance. Similarly, in EGFR-amplified NCH1425 GSCs, EMP3 silencing induced the downregulation of several CDK2 target genes. These include replication-dependent core histones, which are normally transcribed when CDK2 activity peaks at the G1/S boundary of the cell cycle [41, 67]. The mechanism and signaling alterations defined here, while irrelevant for IDH-mutant gliomas that tend to have low EMP3 levels [29, 66], are likely to be broadly applicable to other non-glioma tumor entities, as their RTK signaling outputs have also been shown to be supported by EMP3 [13, 23, 63].

Importantly, our results shed light on how EMP3 can impact oncogenic phenotypes and modulate the outcome of targeted therapies. In line with the observed phosphoproteomic and transcriptomic changes, we show that differentiated EMP3 KO GBM cells have reduced cellular proliferation and blunted mitogenic response to EGF. Furthermore, we demonstrate that EMP3-expressing U-118 and DK-MG cells display lower sensitivities to pan-kinase and EGFR-specific inhibition compared to EMP3 KO cells. In contrast, EMP3 silencing is not sufficient to impair the viability of NCH1425 GSCs, and this may be due to the higher baseline CDK2 activity of and/or additional redundancies that are built within the oncogenic circuits of stem-like cells. However, combining CDK2 inhibition with EMP3 silencing sufficiently compromises the viability of NCH1425 GSCs, highlighting how multiple insults may be required to target stem-like tumor cells. Importantly, EMP3 knockdown potentiates the effect of K03861, indicating that EMP3 can confer resistance against CDK2 inhibition as well. It is well known that GBM cells employ redundant mechanisms to ensure that oncogenic signaling is sustained even after aggressive treatment [24]. By sustaining EGFR/CDK2 activity and by being expressed at such high levels in this tumor entity, EMP3 provides an additional level of resistance that protects tumor cells from targeted kinase inhibitors. This, along with other resistance mechanisms,

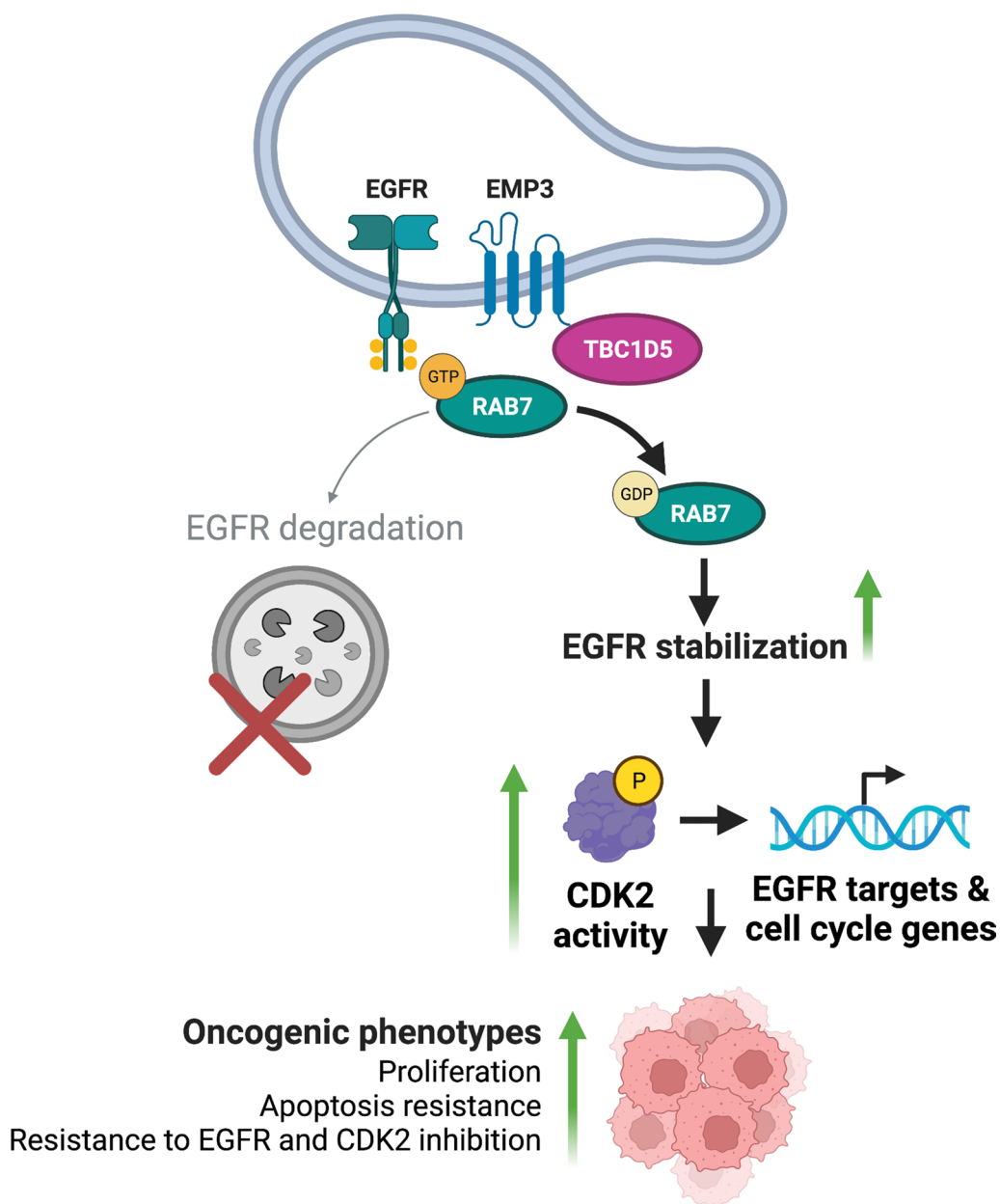


Fig. 9 Proposed model of EMP3 function in GBM. EMP3 interacts with TBC1D5, and the resulting complex inactivates RAB7 in late endosomes. Inactive RAB7 is unable to facilitate EGFR degradation, and EGFR is stabilized. EMP3-dependent stabilization of EGFR sustains downstream signaling via the EGFR effector CDK2. This cascade culminates in the transcription of EGFR-responsive genes involved in cell cycle progression. Ultimately, these mechanisms ensure sustained proliferation, apoptosis resistance, and reduced susceptibility to targeted kinase inhibitors. Figure created with BioRender

could explain why kinase inhibitors have been largely unsuccessful in various clinical trials [47, 56]. It will be worthwhile for future GBM drug discovery screens to explore pharmacological agents that either inhibit EMP3

or synergize with EMP3 silencing. While EMP3 is not a classical oncogene driver, its crucial role in supporting EGFR/CDK2 signaling makes it an appealing addition to traditional somatically altered targets.

Our BioID2-based proximity labeling approach also revealed several other EMP3-proximal proteins, including GBM-relevant membrane receptors (e.g., CD44, integrins, SLCs), signaling adaptors, and other trafficking regulators. This rich dataset provides a wealth of testable hypotheses for future mechanistic investigations on both tumor-intrinsic and tumor-extrinsic effects of EMP3. Given EMP3's emerging role in the tumor immune microenvironment [12] and its high expression in both GBM and tumor-infiltrating macrophages and T cells [46], it would be interesting to investigate how its membrane interactions and/or receptor trafficking function could ultimately influence cancer cell-immune cell crosstalk in GBM. Also of interest is the potential distinct role of glycosylated EMP3, which appears to preferentially associate with inner mitochondrial membrane proteins based on our BioID2 data. Previous studies have shed light on glycan-dependent localization and function of glycosylated mitochondrial proteins [6, 35]. Considering the role of glycosylation in cancer [48], it will be important to investigate the potential role of glycosylated EMP3 in the mitochondria and how it could influence GBM independent of EMP3's effects on EGFR.

In conclusion, this study identifies novel interacting partners of EMP3, thereby highlighting its multi-localizing nature while clarifying the subcellular context in which it could operate as a tumor-promoting protein. Specifically, we unravel a novel EMP3-dependent trafficking mechanism that maintains EGFR activity. By associating with the RAB7 GAP TBC1D5, EMP3 restricts the late endosomal trafficking and inhibits the degradation of activated EGFR receptors. Such a mechanism ensures the maintenance of the EGFR/CDK2 signaling axis, which promotes tumor cell proliferation and provides IDH-wt GBM tumor cells with an additional layer of resistance against targeted EGFR/CDK2 inhibition.

Supplementary Information

The online version contains supplementary material available at <https://doi.org/10.1186/s40478-023-01673-z>.

Additional file 1 Supplementary materials and methods.

Additional file 2. Supplementary figures.

Additional file 3. Perseus analysis of the BioID2 mass spectrometry data.

Additional file 4. Cytoscape annotation of BioID2 hits.

Additional file 5. Mutations identified by whole exome sequencing of GBM cells.

Additional file 6. Perseus analysis of phosphoproteomics MS data.

Additional file 7. Differentially expressed genes in DK-MG and U-118 EMP3 KO vs. controls.

Additional file 8. Differentially expressed genes exclusive to NCH1425 expressing the EMP3 shRNA.

Acknowledgements

We thank Susanne Gärtner and Laura Dörner for the technical assistance and Dr. Julia Zaman, Dr. Peter Angel, and Dr. Francesca Ciccolini for providing valuable feedback on this study. We also thank David Vönhören for his assistance in the Perseus analysis of the phosphoproteomics data. We also thank Dr. Philipp Sievers for assisting with the molecular profiling of the cell lines used in this study. We thank the following core facilities of the DKFZ for their critical support to this study: Antibody, Cellular Tools/Vector and Clone Repository, Light Microscopy, Proteomics, and Microarray. Figures 9 and Additional file 2: Figs. S1 and S4A were created with BioRender.

Author contributions

AAM: Conceptualization; Formal analysis; Investigation; Methodology; Software; Validation; Visualization; Writing—original draft. AK: Investigation; Methodology; Validation; Formal analysis. NB: Investigation; Methodology; Formal analysis. LD: Validation. AC: Methodology; Resources. DK: Methodology; Software. MS: Data curation; Methodology; Software. DH: Data curation; Methodology; Project administration. RW: Methodology. CH: Funding acquisition; Supervision. CH-M: Resources; AvD: Funding acquisition; Supervision; Writing—review and editing. SP: Conceptualization; Funding acquisition; Project administration; Resources; Supervision; Writing—review and editing.

Funding

Open Access funding enabled and organized by Projekt DEAL. This study was supported by doctoral funding provided by the Helmholtz International Graduate School for Cancer Research and SFB 1389—UNITE Glioblastoma grant from the German Research Foundation (Deutsche Forschungsgemeinschaft grant number INST 35/1561-1). The SFB 1389 grant additionally supported Andreas von Deimling and Stefan Pusch.

Availability of data and materials

The data generated in this study are available within the article and its supplementary files.

Declarations

Ethics approval and consent to participate

No consent to participate was required for this study.

Consent for publication

All authors consented to publication.

Competing interests

The authors declare that they have nothing to disclose and have no competing interests related to this work.

Author details

¹Clinical Cooperation Unit (CCU) Neuropathology, German Cancer Research Consortium (DKTK), German Cancer Research Center (DKFZ), Im Neuenheimer Feld 280, 69120 Heidelberg, Germany. ²Department of Neuropathology, Heidelberg University Hospital, Heidelberg, Germany. ³Faculty of Biosciences, Heidelberg University, Heidelberg, Germany. ⁴Faculty of Medicine, Heidelberg University, Heidelberg, Germany. ⁵Present Address: Institute for Molecular Medicine, University Medical Center of the Johannes Gutenberg-University Mainz, Mainz, Germany. ⁶Department of Neuropathology, Institute of Pathology, Hannover Medical School, Hannover, Germany. ⁷Present Address: Canopy Biosciences, Bruker Nano Group, Hannover, Germany. ⁸Light Microscopy Facility, DKFZ, Heidelberg, Germany. ⁹Proteomics Core Facility, DKFZ, Heidelberg, Germany. ¹⁰Cellular Tools Core Facility, DKFZ, Heidelberg, Germany. ¹¹Department of Neurosurgery, Heidelberg University Hospital, Heidelberg, Germany.

Received: 18 April 2023 Accepted: 19 October 2023

Published online: 07 November 2023

References

- Arora M, Moser J, Hoffman TE, Watts LP, Min M, Musteanu M, Rong Y, Ill CR, Nangia V, Schneider J, Sanclemente M, Lapek J, Nguyen L, Niessen S, Dann S, VanArsdale T, Barbacid M, Miller N, Spencer SL (2023) Rapid adaptation to CDK2 inhibition exposes intrinsic cell-cycle plasticity. *Cell* 186:2628–2643.e21. <https://doi.org/10.1016/j.cell.2023.05.013>
- Bakker J, Spits M, Neeffjes J, Berlin I (2017) The EGFR odyssey—from activation to destruction in space and time. *J Cell Sci* 130:4087–4096. <https://doi.org/10.1242/jcs.209197>
- Besson A, Dowdy SF, Roberts JM (2008) CDK inhibitors: cell cycle regulators and beyond. *Dev Cell* 14:159–169. <https://doi.org/10.1016/j.devcel.2008.01.013>
- Borchers A-C, Langemeyer L, Ungermann C (2021) Who's in control? principles of Rab GTPase activation in endolysosomal membrane trafficking and beyond. *J Cell Biol* 220:e202105120. <https://doi.org/10.1083/jcb.202105120>
- Bowman RL, Wang Q, Carro A, Verhaak RGW, Squatrito M (2016) GlioVis data portal for visualization and analysis of brain tumor expression datasets. *Neuro-Oncol* 19:139–141. <https://doi.org/10.1093/neuonc/nov247>
- Burnham-Marusich AR, Berninsone PM (2012) Multiple proteins with essential mitochondrial functions have glycosylated isoforms. *Mitochondrion* 12:423–427. <https://doi.org/10.1016/j.mito.2012.04.004>
- Cardona AF, Jaramillo-Velásquez D, Ruiz-Patiño A, Polo C, Jiménez E, Hakim F, Gómez D, Ramón JF, Cifuentes H, Mejía JA, Salguero F, Ordoñez C, Muñoz Á, Bermúdez S, Useche N, Pineda D, Ricaurte L, Zatarain-Barrón ZL, Rodríguez J, Avila J, Rojas L, Jaller E, Sotelo C, Garcia-Robledo JE, Santoyo N, Rolfo C, Rosell R, Arrieta O (2021) Efficacy of osimertinib plus bevacizumab in glioblastoma patients with simultaneous EGFR amplification and EGFRvIII mutation. *J Neuro-Oncol* 154:353–364. <https://doi.org/10.1007/s11060-021-03834-3>
- Carrasco-García E, Saceda M, Grasso S, Rocamora-Reverte L, Conde M, Gómez-Martínez Á, García-Morales P, Ferragut JA, Martínez-Lacaci I (2011) Small tyrosine kinase inhibitors interrupt EGFR signaling by interacting with erbB3 and erbB4 in glioblastoma cell lines. *Exp Cell Res* 317:1476–1489. <https://doi.org/10.1016/j.yexcr.2011.03.015>
- Casaletto JB, McClatchey AI (2012) Spatial regulation of receptor tyrosine kinases in development and cancer. *Nat Rev Cancer* 12:387–400. <https://doi.org/10.1038/nrc3277>
- Chagoya G, Kwatra SG, Nanni CW, Roberts CM, Phillips SM, Nullmeyergh S, Gilmore SP, Spasojevic I, Corcoran DL, Young CC, Ballman KV, Ramakrishna R, Cross DA, Markert JM, Lim M, Gilbert MR, Lesser GJ, Kwatra MM (2020) Efficacy of osimertinib against EGFRvIII+ glioblastoma. *Oncotarget* 11:2074–2082. <https://doi.org/10.18632/oncotarget.27599>
- Chen H-Z, Tsai S-Y, Leone G (2009) Emerging roles of E2Fs in cancer: an exit from cell cycle control. *Nat Rev Cancer* 9:785–797. <https://doi.org/10.1038/nrc2696>
- Chen Q, Jin J, Huang X, Wu F, Huang H, Zhan R (2021) EMP3 mediates glioblastoma-associated macrophage infiltration to drive T cell exclusion. *J Exp Clin Oncol* 40:160. <https://doi.org/10.1186/s13046-021-01954-2>
- Christians A, Poisel E, Hartmann C, Deimling A, Pusch S (2019) Characterization of the epithelial membrane protein 3 interaction network reveals a potential functional link to mitogenic signal transduction regulation. *Int J Cancer* 145:461–473. <https://doi.org/10.1002/ijc.32107>
- Colman H, Zhang L, Sulman EP, McDonald JM, Shooshtari NL, Rivera A, Popoff S, Nutt CL, Louis DN, Cairncross JG, Gilbert MR, Phillips HS, Mehta MP, Chakravarti A, Pelloski CE, Bhat K, Feuerstein BG, Jenkins RB, Aldape K (2009) A multigene predictor of outcome in glioblastoma. *Neuro-Oncol* 12:49–57. <https://doi.org/10.1093/neuonc/nop007>
- Couturier CP, Ayyadhury S, Le PU, Nadaf J, Monlong J, Riva G, Allache R, Baig S, Yan X, Bourgey M, Lee C, Wang YCD, Yong VW, Guiot M-C, Najafabadi H, Mistic B, Antel J, Bourque G, Ragoussis J, Petrecca K (2020) Single-cell RNA-seq reveals that glioblastoma recapitulates a normal neurodevelopmental hierarchy. *Nat Commun* 11:3406. <https://doi.org/10.1038/s41467-020-17186-5>
- Francavilla C, Papetti M, Rigbolt KTG, Pedersen A-K, Sigurdsson JO, Cazzamali G, Karemire B, Blagoev B, Olsen JV (2016) Multilayered proteomics reveals molecular switches dictating ligand-dependent EGFR trafficking. *Nat Struct Mol Biol* 23:608–618. <https://doi.org/10.1038/nsmb.3218>
- Gani OABSM, Engh RA (2010) Protein kinase inhibition of clinically important staurosporine analogues. *Nat Prod Rep* 27:489–498. <https://doi.org/10.1039/b923848b>
- Gao Y-F, Zhu T, Mao C-X, Liu Z-X, Wang Z-B, Mao X-Y, Li L, Yin J-Y, Zhou H-H, Liu Z-Q (2016) PPIC, EMP3 and CHI3L1 Are novel prognostic markers for high grade glioma. *Int J Mol Sci* 17:1808. <https://doi.org/10.3390/ijms17111808>
- Gullapalli A, Garrett TA, Paing MM, Griffin CT, Yang Y, Trejo J (2004) A role for sorting nexin 2 in epidermal growth factor receptor down-regulation: evidence for distinct functions of sorting nexin 1 and 2 in protein trafficking. *Mol Biol Cell* 15:2143–2155. <https://doi.org/10.1091/mbc.e03-09-0711>
- Guo X, Su J, He X (2019) A 4-gene panel predicting the survival of patients with glioblastoma. *J Cell Biochem* 120:16037–16043. <https://doi.org/10.1002/jcb.28883>
- Harbour ME, Breusegem SYA, Antrobus R, Freeman C, Reid E, Seaman MNJ (2010) The cargo-selective retromer complex is a recruiting hub for protein complexes that regulate endosomal tubule dynamics. *J Cell Sci* 123:3703–3717. <https://doi.org/10.1242/jcs.071472>
- Hebert DN, Lamriben L, Powers ET, Kelly JW (2014) The intrinsic and extrinsic effects of N-linked glycans on glycoproteostasis. *Nat Chem Biol* 10:902–910. <https://doi.org/10.1038/nchembio.1651>
- Hsieh Y-H, Hsieh S-C, Lee C-H, Yang S-F, Cheng C-W, Tang M-J, Lin C-L, Lin C-L, Chou R-H (2015) Targeting EMP3 suppresses proliferation and invasion of hepatocellular carcinoma cells through inactivation of PI3K/Akt pathway. *Oncotarget* 6:34859–34874. <https://doi.org/10.18632/oncotarget.5414>
- Huang PH, Xu AM, White FM (2009) Oncogenic EGFR signaling networks in glioma. *Sci Signal* 2:re6. <https://doi.org/10.1126/scisignal.287re6>
- Huotari J, Helenius A (2011) Endosome maturation. *Embo J* 30:3481–3500. <https://doi.org/10.1038/emboj.2011.286>
- Jänne PA, Yang JC-H, Kim D-W, Planchard D, Ohe Y, Ramalingam SS, Ahn M-J, Kim S-W, Su W-C, Horn L, Haggstrom D, Felip E, Kim J-H, Frewer P, Cantarini M, Brown KH, Dickinson PA, Giorghiu S, Ranson M (2015) AZD9291 in EGFR inhibitor-resistant non-small-cell lung cancer. *New Engl J Med* 372:1689–1699. <https://doi.org/10.1056/nejmoa1411817>
- Jia D, Zhang J-S, Li F, Wang J, Deng Z, White MA, Osborne DG, Phillips-Krawczak C, Gomez TS, Li H, Singla A, Burstein E, Billadeau DD, Rosen MK (2016) Structural and mechanistic insights into regulation of the retromer coat by TBC1d5. *Nat Commun* 7:13305. <https://doi.org/10.1038/ncomms13305>
- Jimenez-Orgaz A, Kvainickas A, Nägele H, Denner J, Eimer S, Dengjel J, Steinberg F (2018) Control of RAB7 activity and localization through the retromer-TBC1D5 complex enables RAB7-dependent mitophagy. *Embo J* 37:235–254. <https://doi.org/10.15252/emboj.201797128>
- Jun F, Hong J, Liu Q, Guo Y, Liao Y, Huang J, Wen S, Shen L (2016) Epithelial membrane protein 3 regulates TGF- β signaling activation in CD44-high glioblastoma. *Oncotarget*. <https://doi.org/10.18632/oncotarget.11102>
- Kim DJ, Jensen SC, Noble KA, KC B, Roux KH, Motamedchaboki K, Roux KJ (2016) An improved smaller biotin ligase for BioID proximity labeling. *Mol Biol Cell* 27:1188–1196. <https://doi.org/10.1091/mbc.e15-12-0844>
- Knight JDR, Choi H, Gupta GD, Pelletier L, Raught B, Nesvizhskii AI, Gingras A-C (2017) ProHits-viz: a suite of web tools for visualizing interaction proteomics data. *Nat Methods* 14:645–646. <https://doi.org/10.1038/nmeth.4330>
- Kobayashi S, Shimamura T, Monti S, Steidl U, Hetherington CJ, Lowell AM, Golub T, Meyerson M, Tenen DG, Shapiro GI, Halmos B (2006) Transcriptional profiling identifies cyclin D1 as a critical downstream effector of mutant epidermal growth factor receptor signaling. *Cancer Res* 66:11389–11398. <https://doi.org/10.1158/0008-5472.can-06-2318>
- Koff A, Giordano A, Desai D, Yamashita K, Harper JW, Elledge S, Nishimoto T, Morgan DO, Franza BR, Roberts JM (1992) Formation and activation of a cyclin E-cdk2 complex during the G1 phase of the human cell cycle. *Science* 257:1689–1694. <https://doi.org/10.1126/science.1388288>
- Kuleshov MV, Xie Z, London ABK, Yang J, Evangelista JE, Lachmann A, Shu I, Torre D, Ma'ayan A (2021) KEA3: improved kinase enrichment analysis via data integration. *Nucleic Acids Res* 49:W304–W316. <https://doi.org/10.1093/nar/gkab359>
- Kung LA, Tao S-C, Qian J, Smith MG, Snyder M, Zhu H (2009) Global analysis of the glycoproteome in *Saccharomyces cerevisiae* reveals new roles for

- protein glycosylation in eukaryotes. *Mol Syst Biol* 5:308–308. <https://doi.org/10.1038/msb.2009.64>
36. Kurten RC, Cadena DL, Gill GN (1996) Enhanced degradation of EGF receptors by a sorting nexin, SNX1. *Science* 272:1008–1010. <https://doi.org/10.1126/science.272.5264.1008>
 37. Kvainickas A, Nägele H, Qi W, Dokládal L, Jimenez-Organ A, Stehl L, Gangurde D, Zhao Q, Hu Z, Dengjel J, Virgilio CD, Baumeister R, Steinberg F (2019) Retromer and TBC1D5 maintain late endosomal RAB7 domains to enable amino acid–induced mTORC1 signaling. *Retromer maintains amino acid signaling*. *J Cell Biol* 218:3019–3038. <https://doi.org/10.1083/jcb.201812110>
 38. Liu H, Weng J (2022) A comprehensive bioinformatic analysis of cyclin-dependent kinase 2 (CDK2) in glioma. *Gene* 822:146325. <https://doi.org/10.1016/j.gene.2022.146325>
 39. Liu X, Chen X, Shi L, Shan Q, Cao Q, Yue C, Li H, Li S, Wang J, Gao S, Niu M, Yu R (2019) The third-generation EGFR inhibitor AZD9291 overcomes primary resistance by continuously blocking ERK signaling in glioblastoma. *J Exp Clin Cancer Res* 38:219. <https://doi.org/10.1186/s13046-019-1235-7>
 40. Louis DN, Perry A, Wesseling P, Brat DJ, Cree IA, Figarella-Branger D, Hawkins C, Ng HK, Pfister SM, Reifenberger G, Soffietti R, von Deimling A, Ellison DW (2021) The 2021 WHO classification of tumors of the central nervous system: a summary. *Neuro-Oncol* 23:1231–1251. <https://doi.org/10.1093/neuonc/noab106>
 41. Ma T, Tine BAV, Wei Y, Garrett MD, Nelson D, Adams PD, Wang J, Qin J, Chow LT, Harper JW (2000) Cell cycle–regulated phosphorylation of p220NPAT by cyclin E/Cdk2 in Cajal bodies promotes histone gene transcription. *Genes Dev* 14:2298–2313. <https://doi.org/10.1101/gad.829500>
 42. Maddika S, Ande SR, Wiechec E, Hansen LL, Wesselborg S, Los M (2008) Akt-mediated phosphorylation of CDK2 regulates its dual role in cell cycle progression and apoptosis. *J Cell Sci* 121:979–988. <https://doi.org/10.1242/jcs.009530>
 43. Martija AA, Pusch S (2021) The multifunctional role of EMP3 in the regulation of membrane receptors associated with IDH-Wild-Type glioblastoma. *Int J Mol Sci* 22:5261. <https://doi.org/10.3390/ijms22105261>
 44. McLendon R, Friedman A, Bigner D, Meir EGV, Brat DJ, Mastrogianakis GM, Olson JJ, Mikkelsen T, Lehman N, Aldape K, Yung WKA, Bogler O, Vandenberg S, Berger M, Prados M, Muzny D, Morgan M, Scherer S, Sabo A, Nazareth L, Lewis L, Hall O, Zhu Y, Ren Y, Alvi O, Yao J, Hawes A, Jhangiani S, Fowler G, Lucas AS, Kovar C, Cree A, Dinh H, Santibanez J, Joshi V, Gonzalez-Garay ML, Miller CA, Milosavljevic A, Donehower L, Wheeler DA, Gibbs RA, Cibulskis K, Sougnez C, Fennell T, Mahan S, Wilkinson J, Ziaugra L, Onofrio R, Bloom T, Nicol R, Ardlie K, Baldwin J, Gabriel S, Lander ES, Ding L, Fulton RS, McLellan MD, Wallis J, Larson DE, Shi X, Abbott R, Fulton L, Chen K, Koboldt DC, Wendl MC, Meyer R, Tang Y, Lin L, Osborne JR, Dunford-Shore BH, Miner TL, Delehaunty K, Markovic C, Swift G, Courtney W, Pohl C, Abbott S, Hawkins A, Leong S, Haipek C, Schmidt H, Wiechert M, Vickery T, Scott S, Dooling DJ, Chinwalla A, Weinstock GM, Mardis ER, Wilson RK, Getz G, Winckler W, Verhaak RGW, Lawrence MS, O’Kelly M, Robinson J, Alexe G, Beroukchim R, Carter S, Chiang D, Gould J, Gupta S, Korn J, Mermel C, Mesirov J, Monti S, Nguyen H, Parkin M, Reich M, Stransky N, Weir BA, Garraway L, Golub T, Meyerson M, Chin L, Protopopov A, Zhang J, Perna I, Aronson S, Sathiamoorthy N, Ren G, Yao J, Wiedemeyer WR, Kim H, Kong SW, Xiao Y, Kohane IS, Seidman J, Park PJ, Kucherlapati R, Laird PW, Cope L, Herman JG, Weisenberger DJ, Pan F, Berg DVD, Nesterov LV, Yi JM, Schuebel KE, Bayliss SB, Absher DM, Li JZ, Southwick A, Brady S, Aggarwal A, Chung T, Sherlock G, Brooks JD, Myers RM, Spellman PT, Purdom E, Jakkula LR, Lapuk AV, Marr H, Dorton S, Choi YG, Han J, Ray A, Wang V, Durinck S, Robinson M, Wang NJ, Vranizan K, Peng V, Name EV, Fontenay GV, Ngai J, Conboy JG, Parvin B, Feiler HS, Speed TP, Gray JW, Brennan C, Socci ND, Olshen A, Taylor BS, Lash A, Schultz N, Reva B, Antipin Y, Stukalov A, Gross B, Cerami E, Wang WQ, Qin L-X, Seshan VE, Villafania L, Cavatore M, Borsu L, Viale A, Gerald W, Sander C, Ladanyi M, Perou CM, Hayes DN, Topal MD, Hoadley KA, Qi Y, Balu S, Shi Y, Wu J, Penny R, Bittner M, Shelton T, Lenkiewicz E, Morris S, Beasley D, Sanders S, Kahn A, Sfeir R, Chen J, Nassau D, Feng L, Hickey E, Zhang J, Weinstein JN, Barker A, Gerhard DS, Vockley J, Compton C, Vaught J, Fielding P, Ferguson ML, Schaefer C, Madhavan S, Buetow KH, Collins F, Good P, Guyer M, Ozenberger B, Peterson J, Thomson E (2008) Comprehensive genomic characterization defines human glioblastoma genes and core pathways. *Nature* 455:1061–1068. <https://doi.org/10.1038/nature07385>
 45. Mesosson Y, Mills GB, Yarden Y (2008) Derailed endocytosis: an emerging feature of cancer. *Nat Rev Cancer* 8:835–850. <https://doi.org/10.1038/nrc2521>
 46. Neftel C, Laffy J, Filbin MG, Hara T, Shore ME, Rahme GJ, Richman AR, Silverbush D, Shaw ML, Hebert CM, Dewitt J, Gritsch S, Perez EM, Castro LNG, Lan X, Druck N, Rodman C, Dionne D, Kaplan A, Bertalan MS, Small J, Pelton K, Becker S, Bonal D, Nguyen Q-D, Servis RL, Fung JM, Mylvaganam R, Mayr L, Gojo J, Haberler C, Geyeregger R, Czech T, Slavic I, Nahed BV, Curry WT, Carter BS, Wakimoto H, Brastianos PK, Batchelor TT, Stemmer-Rachamimov A, Martinez-Lage M, Frosch MP, Stamenkovic I, Riggi N, Rheinbay E, Monje M, Rozenblatt-Rosen O, Cahill DP, Patel AP, Hunter T, Verma IM, Ligon KL, Louis DN, Regev A, Bernstein BE, Tirosh I, Suvà ML (2019) An integrative model of cellular states, plasticity, and genetics for glioblastoma. *Cell* 178:835–849.e21. <https://doi.org/10.1016/j.cell.2019.06.024>
 47. Pearson JRD, Regad T (2017) Targeting cellular pathways in glioblastoma multiforme. *Signal Transduct Target Ther* 2:17040. <https://doi.org/10.1038/sigtrans.2017.40>
 48. Pinho SS, Reis CA (2015) Glycosylation in cancer: mechanisms and clinical implications. *Nat Rev Cancer* 15:540–555. <https://doi.org/10.1038/nrc3982>
 49. Rappsilber J, Mann M, Ishihama Y (2007) Protocol for micro-purification, enrichment, pre-fractionation and storage of peptides for proteomics using StageTips. *Nat Protoc* 2:1896–1906. <https://doi.org/10.1038/nprot.2007.261>
 50. Ruprecht B, Koch H, Domasinska P, Frejno M, Kuster B, Lemeer S (2017) Optimized enrichment of phosphoproteomes by Fe-IMAC column chromatography. *Methods Mol Biol Clifton N J* 1550:47–60. https://doi.org/10.1007/978-1-4939-6747-6_5
 51. Schindler C, Chen Y, Pu J, Guo X, Bonifacino JS (2015) EARP is a multi-subunit tethering complex involved in endocytic recycling. *Nat Cell Biol* 17:639–650. <https://doi.org/10.1038/ncb3129>
 52. Seaman MNJ, Harbour ME, Tattersall D, Read E, Bright N (2009) Membrane recruitment of the cargo-selective retromer subcomplex is catalysed by the small GTPase Rab7 and inhibited by the Rab-GAP TBC1D5. *J Cell Sci* 122:2371–2382. <https://doi.org/10.1242/jcs.048686>
 53. Seaman MNJ, Mukadam AS, Breusegem SY (2018) Inhibition of TBC1D5 activates Rab7a and can enhance the function of the retromer cargo-selective complex. *J Cell Sci* 131:jcs.217398. <https://doi.org/10.1242/jcs.217398>
 54. Shannon P, Markiel A, Ozier O, Baliga NS, Wang JT, Ramage D, Amin N, Schwikowski B, Ideker T (2003) Cytoscape: a software environment for integrated models of biomolecular interaction networks. *Genome Res* 13:2498–2504. <https://doi.org/10.1101/gr.1239303>
 55. Shrimall S, Cherepanova NA, Gilmore R (2015) Cotranslational and post-translational N-glycosylation of proteins in the endoplasmic reticulum. *Semin Cell Dev Biol* 41:71–78. <https://doi.org/10.1016/j.semdb.2014.11.005>
 56. Silva ECD, Mercier M-C, Etienne-Selloum N, Dontenwill M, Choulier L (2021) A systematic review of glioblastoma-targeted therapies in phases II, III IV clinical trials. *Cancers* 13:1795. <https://doi.org/10.3390/cancers13081795>
 57. Subramanian A, Tamayo P, Mootha VK, Mukherjee S, Ebert BL, Gillette MA, Paulovich A, Pomeroy SL, Golub TR, Lander ES, Mesirov JP (2005) Gene set enrichment analysis: a knowledge-based approach for interpreting genome-wide expression profiles. *Proc Natl Acad Sci* 102:15545–15550. <https://doi.org/10.1073/pnas.0506580102>
 58. Thul PJ, Åkesson L, Wiking M, Mahdavian D, Geladaki A, Blal HA, Alm T, Asplund A, Björk L, Breckels LM, Bäckström A, Danielsson F, Fagerberg L, Fall J, Gatto L, Gnann C, Hober S, Hjelmare M, Johansson F, Lee S, Lindskog C, Mulder J, Mulvey CM, Nilsson P, Oksvold P, Rockberg J, Schütten R, Schwenk JM, Sivertsson Å, Sjöstedt E, Skogs M, Stadler C, Sullivan DP, Tegel H, Winsnes C, Zhang C, Zwahlen M, Mardinoglu A, Pontén F, von Feilitzen K, Lilley KS, Uhlén M, Lundberg E (2017) A subcellular map of the human proteome. *Science* 356:eaal3321. <https://doi.org/10.1126/science.aal3321>

59. Tyanova S, Temu T, Cox J (2016) The MaxQuant computational platform for mass spectrometry-based shotgun proteomics. *Nat Protoc* 11:2301–2319. <https://doi.org/10.1038/nprot.2016.136>
60. Tyanova S, Temu T, Sinitcyn P, Carlson A, Hein MY, Geiger T, Mann M, Cox J (2016) The Perseus computational platform for comprehensive analysis of (prote)omics data. *Nat Methods* 13:731–740. <https://doi.org/10.1038/nmeth.3901>
61. Varn FS, Johnson KC, Martinek J, Huse JT, Nasrallah MP, Wesseling P, Cooper LAD, Malta TM, Wade TE, Sabedot TS, Brat D, Gould PV, Wöehr A, Aldape K, Ismail A, Sivajothi SK, Barthel FP, Kim H, Kocakavuk E, Ahmed N, White K, Datta I, Moon H-E, Pollock S, Goldfarb C, Lee G-H, Garofano L, Anderson KJ, Nehar-Belaid D, Barnholtz-Sloan JS, Bakas S, Byrne AT, D'Angelo F, Gan HK, Khasraw M, Migliozi S, Ormond DR, Paek SH, Meir EGV, Walenkamp AME, Watts C, Weiss T, Weller M, Palucka K, Stead LF, Poisson LM, Noushmehr H, Iavarone A, Verhaak RGW, Alfaro KD, Amin SB, Ashley DM, Bock C, Brodbelt A, Bulsara KR, Castro AV, Connelly JM, Costello JF, de Groot JF, Finocchiaro G, French PJ, Golebiewska A, Hau AC, Hong C, Horbinski C, Kannan KS, Kouwenhoven MC, Lasorella A, LaViolette PS, Ligon KL, Lowman AK, Mehta S, Miletic H, Molinaro AM, Ng HK, Niclou SP, Niers JM, Phillips JJ, Rabadan R, Rao G, Reifensberger G, Sanai N, Short SC, Smitt PS, Sloan AE, Smits M, Snyder JM, Suzuki H, Tabatabai G, Tanner G, Tomaszewski WH, Wells M, Westerman BA, Wheeler H, Xie J, Yung WKA, Zadeh G, Zhao J, Verhaak RG (2022) Glioma progression is shaped by genetic evolution and microenvironment interactions. *Cell* 185:2184–2199.e16. <https://doi.org/10.1016/j.cell.2022.04.038>
62. Wang J, Yang T, Xu G, Liu H, Ren C, Xie W, Wang M (2016) Cyclin-dependent kinase 2 promotes tumor proliferation and induces radio resistance in glioblastoma. *Transl Oncol* 9:548–556. <https://doi.org/10.1016/j.tranon.2016.08.007>
63. Wang Y-W, Li W-M, Wu W-J, Chai C-Y, Liu H-S, Lai M-D, Chow N-H (2014) Potential significance of EMP3 in patients with upper urinary tract urothelial carcinoma: crosstalk with ErbB2-PI3K-Akt pathway. *J Urol* 192:242–251. <https://doi.org/10.1016/j.juro.2013.12.001>
64. Wessel D, Flügge UI (1984) A method for the quantitative recovery of protein in dilute solution in the presence of detergents and lipids. *Anal Biochem* 138:141–143. [https://doi.org/10.1016/0003-2697\(84\)90782-6](https://doi.org/10.1016/0003-2697(84)90782-6)
65. Yilmaz S, Ayati M, Schlatzer D, Çiçek AE, Chance MR, Koyutürk M (2021) Robust inference of kinase activity using functional networks. *Nat Commun* 12:1177. <https://doi.org/10.1038/s41467-021-21211-6>
66. Yue H, Xu Q, Xie S (2018) High EMP3 expression might independently predict poor overall survival in glioblastoma and its expression is related to DNA methylation. *Medicine* 97:e9538. <https://doi.org/10.1097/md.00000000000009538>
67. Zhao J, Kennedy BK, Lawrence BD, Barbie DA, Matera AG, Fletcher JA, Harlow E (2000) NPAT links cyclin E-Cdk2 to the regulation of replication-dependent histone gene transcription. *Genes Dev* 14:2283–2297. <https://doi.org/10.1101/gad.827700>
68. Zhong Q, Lazar CS, Tronchère H, Sato T, Meerloo T, Yeo M, Songyang Z, Emr SD, Gill GN (2002) Endosomal localization and function of sorting nexin 1. *Proc Natl Acad Sci* 99:6767–6772. <https://doi.org/10.1073/pnas.092142699>

Publisher's Note

Springer Nature remains neutral with regard to jurisdictional claims in published maps and institutional affiliations.

Ready to submit your research? Choose BMC and benefit from:

- fast, convenient online submission
- thorough peer review by experienced researchers in your field
- rapid publication on acceptance
- support for research data, including large and complex data types
- gold Open Access which fosters wider collaboration and increased citations
- maximum visibility for your research: over 100M website views per year

At BMC, research is always in progress.

Learn more biomedcentral.com/submissions

